UNIVERSIDAD DE CHILE
FACULTAD DE CIENCIAS FÍSICAS Y MATEMÁTICAS
DEPARTAMENTO DE INGENIERÍA MECÁNICA

NUMERICAL SIMULATION OF HEAT TRANSFER ENHANCEMENT IN FIN AND TUBE COMPACT HEAT EXCHANGER WITH LONGITUDINAL VORTEX GENERATOR

MEMORIA PARA OPTAR AL TÍTULO DE INGENIERA CIVIL MECÁNICA

KATHERINE ODETTE BARQUIN TRUJILLO

PROFESOR GUÍA:
ÁLVARO VALENCIA MUSALEM

MIEMBROS DE LA COMISIÓN:
WILLIAMS CALDERÓN MUÑOZ
RAMÓN FREDERICK GONZÁLEZ

SANTIAGO, CHILE
2020

RESUMEN DE LA MEMORIA PARA OPTAR
AL TÍTULO DE INGENIERA CIVIL MECÁNICA
POR: KATHERINE ODETTE BARQUIN TRUJILLO
FECHA: 2020
PROF. GUÍA: ÁLVARO VALENCIA MUSALEM

NUMERICAL SIMULATION OF HEAT TRANSFER ENHANCEMENT IN FIN AND TUBE COMPACT HEAT EXCHANGER WITH LONGITUDINAL VORTEX GENERATOR

Over the last decades several studies have searched for improved Tube and Fin Heat Exchanger (TFHE) designs capable of providing the best thermohydraulic performance at the lowest possible cost. Such studies have proven relevant due to the various domestic and industrial applications of TFHEs. In order to enhance the heat transfer rate, they emphasize the use of passive methods involving the implementation of different types of Vortex Generators (VGs) and tubes, as well as their arrangements and parameters.

Every research has suggested at least one new configuration for TFHE; therefore, the number of available studies is large. In fact, each proposed configuration is composed of different parameters and arrangements for Heat Exchangers (HEs), tubes and VGs. This is why they cannot be compared. The present study aims at quantifying and comparing the thermohydraulic performance of HE configurations that were recognized as successful at enhancing heat transfer in previous research. Six new designs were proposed, all of them with identical parameters so they could be compared. Each design presented a more complex configuration than the previous one. The first case consisted of an in-line circular tube arrangement and the last one was a staggered oval tube with two pairs of Delta Winglet Vortex Generators (DWVGs) in CFU-CFD orientation.

Designing a validation model was key to achieving the objectives of this study and ensuring an appropriate procedure leading to appropriate results. For achieving this purpose, the heat transfer coefficient and friction factor were compared with a previous study. Once the model was validated and the grid independence was achieved, six different designs based on previous research were proposed. These TFHEs configurations were simulated and their flow behaviours were analysed.

Their performance was compared based on the Nusselt number and the friction factors obtained. Every geometry showed a better performance than the preceding design. Superior performances were achieved with lower Reynolds and the best performance was observed in the HE with staggered oval tubes and two pairs of DWVGs in CFU-CFD orientation (Case 5), the last configuration proposed. This configuration in particular enabled a 90% increase of the thermal performance factor when compared with the base case.

Every new design had a better performance than the previous one: staggered tubes improved the flow mix in dead water zones, oval tubes presented a smaller stagnation zone and DWVGs interrupted boundary layers. The sum of all of these implies a better performance.

RESUMEN DE LA MEMORIA PARA OPTAR
AL TÍTULO DE INGENIERA CIVIL MECÁNICA
POR: KATHERINE ODETTE BARQUIN TRUJILLO
FECHA: 2020
PROF. GUÍA: ÁLVARO VALENCIA MUSALEM

NUMERICAL SIMULATION OF HEAT TRANSFER ENHANCEMENT IN FIN AND TUBE COMPACT HEAT EXCHANGER WITH LONGITUDINAL VORTEX GENERATOR

Durante las últimas décadas, varios estudios han buscado diseños mejorados de intercambiadores de calor de tubos y aletas (TFHE) capaces de proporcionar el mejor rendimiento termohidráulico al menor costo posible. Dichos estudios son relevantes debido a las diversas aplicaciones domésticas e industriales de los TFHE. Para mejorar la tasa de transferencia de calor, enfatizan el uso de métodos pasivos que involucran la implementación de diferentes tipos de generadores de vórtice (VG) y tubos, así como sus disposiciones y parámetros.

Cada investigación ha sugerido al menos una nueva configuración para TFHE; por lo tanto, el número de estudios disponibles es grande. De hecho, cada configuración propuesta se compone de diferentes parámetros y disposiciones para intercambiadores de calor (HE), tubos y VG. Por eso, entre ellos, no son comparables. El presente estudio tiene como objetivo cuantificar y comparar el rendimiento termohidráulico de configuraciones de HEs que demostraron un desempeño superior en cuanto al aumento de transferencia de calor en investigaciones anteriores. Se propusieron seis nuevos diseños, todos ellos con idénticos parámetros para poder ser comparados. Cada diseño presentaba una configuración más compleja que el anterior. El primer caso consistió en bancos de tubos circulares en línea y el último consistió en tubos ovalados desplazados con dos pares de generadores de vórtices Delta Winglet (DWVG) en orientación CFU-CFD.

El diseño de un modelo de validación fue clave para lograr los objetivos de este estudio y garantizar un procedimiento apropiado que conduzca a resultados adecuados. Para lograr este propósito, se comparó el coeficiente de transferencia de calor y el factor de fricción con los resultados obtenidos por una investigación con características similares. Una vez que el modelo fue validado y la independencia del mallado fue demostrada, se propusieron seis diseños diferentes basados en investigaciones previas. Estas configuraciones de TFHE se simularon y finalmente se analizaron los comportamientos del flujo.

Su desempeño se comparó en base al número de Nusselt y los factores de fricción obtenidos. Se lograron rendimientos superiores con Reynolds más bajos y el mejor desempeño se observó en el HE con tubos ovalados desplazados y dos pares de DWVGs en orientación CFU-CFD (Caso 5), la última configuración propuesta. Esta configuración en particular permitió un aumento del 90 % del factor de rendimiento térmico en comparación con el caso base.

Cada nuevo diseño tuvo un mejor rendimiento que el anterior: los tubos desplazados mejoraron la mezcla en las zonas de agua muerta, los tubos ovalados presentaron una menor zona de estancamiento y los DWVG interrumpieron las capas límite. La suma de todos estos implica un mejor desempeño.

Muy frío, no habíamos visto un frío tanto este año como este año tanto frío.

Acknowledgment

Primero que todo quiero agradecer a mi familia por apoyarme a lo largo de mi vida universitaria especialmente a mis abuelos por permitirme estar en su casa durante mi periodo de estudio. Papá, gracias por brindarme lo que he necesitado estos años. Mamá, si antes no lo sabias, quiero que sepas que eres la mujer más fuerte que he conocido y un ejemplo a seguir para mi, gracias por tanto.

Agradezco a las personas con quienes coincidí durante la universidad. El mítico amigue, conocerte es un privilegio, traes luz solo que aún no te has dado cuenta. Tiare, gracias a ti por volver a poner mis pies en tierra y levantarme cuando más lo necesité. Dani, eres brillante, quien trabaje contigo lo apreciará, eres inspiración. Papo, gracias por compartir aprendizajes no solo universitarios conmigo. Muchas gracias a la gente bonita del cuarto: Coni, Mauro, Francis, Suelto, Nico, Cata y Oveja. Es difícil encontrar un grupo con tanto apañe incondicional. Gracias a los cabros: Viki, Marco, Nico, Edu, Benja, Jota, Mati, Claudio, Lucas, Camilo y Cristian. Las tardes de juego, películas y salidas no se olvidan, espero poder seguir compartiendo con todos, los quiero mucho.

Este año conocí gente maravillosa. Tati, eres una mujer talentosa y muy inteligente, gracias por confiar en mi, retarme más de una vez si es necesario, darme ánimos y compartir mucho más que gatos, espero pronto te veas con mis ojos y entiendas lo mucho que vales. Nano, solo bastaba una tesis que nos juntara para que todo lo demás cayera en su lugar, gracias por estar ahí y quiero que sepas que también estaré para ti. Fernando, tu apoyo ha sido incondicional, no sé cómo agradecer los buenos ratos y palabras de aliento, muchas gracias. Felipe, gracias por haber estado, por inspirarme a ir por más, no sabes el impacto que tuviste en mi vida, siempre estaré muy agradecida.

Gracias a mis amigos Diego, Popín y Julio, siempre que vuelvo a Concepción me siento en casa al verlos, aunque pasen los años al estar con ustedes todo es como siempre. Pablo, el mejor ex, gracias por acompañarme y compartir tus consejos, conversar contigo es un aprendizaje continuo.

Muchas gracias a mi profesor guía Alvaro Valencia, por la ayuda constante y las palabras de aliento. Gracias a Claudia Villarreal, por ayudarme con cada percance a lo largo de mi paso por Mecánica, siempre la recuerdo con una sonrisa. Y gracias al profesor Aquiles por su preocupación, su llamada significó mucho para mi.

Finalmente quiero agradecer a mi gata Canela mi compañera de estudio nocturno, quien me enseñó todo lo que sé, te amo mi gorda.

Nomenclature

A_c	Minimum Cross Sectional Area, m^2
A_0	Total Surface Area, m^2
C_p	Specific Heat, J kg^{-1} K^{-1}
D_h	Hydraulic Diameter, m
D	Fin Collar Outside Diameter, m
f	Friction Factor
F_p	Fin Pitch, m
F_t	Fin Thickness, m
h	Heat Transfer Coefficient, W m^{-2} K^{-1}
JF_w	Thermal performance factor
k_{air}	Air Conductivity, W m^{-1} K^{-1}
L	Air Flow Direction Length, m
LMTD	Logarithmic-Mean Temperature Difference , K
L_p	Longitudinal Pitch, m
$\dot{m}$	Mass Flow, kg s^{-1}
Nu_{local}	Local Nusselt Number
Nu_{sp}	Span Average Nusselt Number
Nu_a	Average Nusselt Number
p	Total Pressure, Pa
p_a	Area-Average Pressure, Pa
Q	Heat Transfer Rate, W
q	Heat Flux, W m^{-2}
Re	Reynolds Number
T_{bulk}	Bulk Temperature, K
T_{fin}	Temperature of the Fin, K
T_{in}	Inlet Temperature, K
T_{out}	Outlet Temperature, K
T_p	Transverse Pitch, m
T_{wall}	Wall Temperature, K
U_c	Velocity at the Minimum Cross-Section Area, m s^{-1}
U_{in}	Inlet Velocity, m s^{-1}
u, v, w	Velocity Components in x-,y-,z- directions, m s^{-1}

Acronyms

CFD	Common-Flow Down
CFU	Common-Flow Up
CHE	Compact Heat Exhanger
DWVG	Delta Winglet Vortex Generators
HE	Heat Exchanger
LVG	Longitudinal Vortices Generator
TFHE	Tube and Fin Heat Exchanger
TVG	Transverse Vortices Generator
VG	Vortices Generator

Greek Symbols

ΔP	Pressure Difference, Pa
μ	Absolute Viscosity of Air, kg m^{-1} s^{-1}
ρ	Air Density, kg m^{-3}

Contents

Table Index

Illustration Index

Chapter 1

Introduction

Because of their various applications, from domestic to industrial, HEs have been studied for decades. They consist of heat transfer devices that exchange heat between two or more fluids. Depending on their applications, construction features, surface compactness and transfer processes, many different types of HEs can be found.

TFHEs work with two fluids, commonly air and water which runs through the tube, exchanging heat through the tube wall by conduction. TFHEs are used in air conditioning, refrigeration, among other applications, due to their reduced size and weight, also known as compactness. The latter is enhanced either by means of fins on the air side or the fluid with the lowest heat transfer coefficient. This improves the heat transfer rate by increasing the surface area. This is just one of many passive mechanisms employed to enhance heat transfer.

Another way of increasing the heat transfer rate in TFHEs is to achieve a better fluid mix and flow destabilization through vortices developed by VGs located on the air side. Longitudinal Vortex Generators (LVG) have shown a better performance than transverse vortex generators (TVG) given that longitudinal vortices last over long distances. Aspects such as geometric parameters, type of LVG and inlet velocity have a direct impact on vortex strength.

In fact, modifying the design of heat exchangers as well as the geometric parameters, position and type of VG and tube has an impact on heat transfer and pressure loss. This is currently a matter of interest for several studies searching for the best thermohydraulic performance at the lowest cost.

1.1. Motivation

Event though there is a large number of studies examining this subject, they cannot be compared because of the heat exchanger specificities and the different parameters and arrangements of the tube and VG. The purpose of this study is to quantify heat transfer enhancement and pressure loss in the design of heat exchangers using the same parameters so comparisons can be established. The proposed designs will be based on arrangements found in studies showing a superior performance. Moreover, the configuration of each design will be more complex than the previous one.

1.2. Objectives

Quantify and compare the thermohydraulic performance of 6 designs of TFHE with delta winglet LVG type.

1.2.1. Specific Objectives

- Design TFHEs based on previous studies.
- Identify effects on the flow behaviour and thermal performance relating to each of the new TFHE designs proposed in this study.

1.3. Scope of this study

This research constitutes a numerical study in which the software ANSYS fluent was used and was focused on the air side (exterior zone) of the TFHE.

- Six different TFHE designs were analyzed. The complexity of the configurations varied with each new design, the last being the most complex of all. The first arrangement consisted of three in-line circular tubes, and the last one corresponded to staggered oval tubes with two pairs of DWVGs.
- For each case, five simulations were solved using different Reynolds numbers ranging from 500 to 2500. Due to low Reynolds, laminar flow was considered.
- The comparison criteria were Nusselt number and friction factor.

Chapter 2

Literature Review

2.1. Heat Exchangers

HEs consist of devices that exchange heat between two or more fluids. Numerous industries and households use them in processes requiring the heating or cooling of a fluid for different purposes. Some examples of HEs are cooling towers, shell-and-tube exchangers, automobile radiators, condenser and evaporators. A great number of HEs has been developed. They can be classified according to transfer processes, number of fluids, surface compactness, construction features, flow arrangement, heat transfer mechanisms and applications [1].

Regarding compactness, it is worth mentioning that when the area density of HEs —the ratio between the heat transfer surface area and the volume of the HE— is greater than 700 m^2/m^3, then it is considered as an extended surface HE or compact HE (CHE). CHEs are widely used in air conditioning and refrigeration because of their reduced weight and size. One way to increase the area density is to add fins to the HE. For example, in gas-to-liquid HE, the heat transfer coefficient on the liquid side is generally one order of magnitude higher than the gas side. Therefore, to balance the thermal conductance for a minimum-size HE, fins need to be on the air side to reach a major surface area, and consequently, a larger heat transfer area [1][2].

TFHEs are one of the most common types of CHE. They consist of a HE in which the heat transfer occurs between two fluids by conduction through a tube wall. Commonly, this type of HE uses fins on the air side to enhance compactness. The tubes can be individually finned or share one single continuous larger fin, as Figure 2.1 shows. TFHEs can withstand high pressures on the tube side, and the operating temperature is limited by the type of bonding, materials employed and material thickness. Due to these characteristics, they are used in air-conditioning, refrigeration, airplanes, automobiles, heat pumps, among many other applications [1][2].

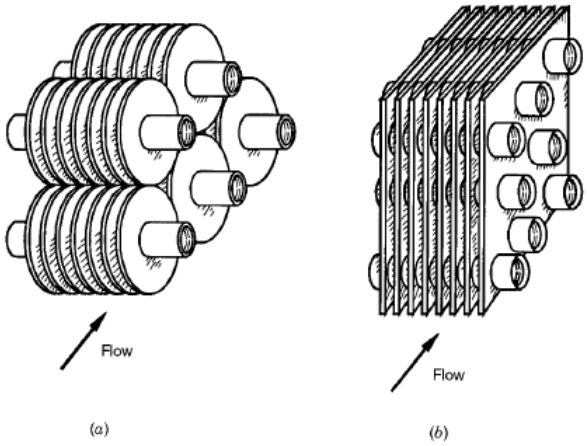

Figure 2.1: Finned tubes designs [2].

2.2. Longitudinal Vortex Generators

Fins and VGs are employed as a way of increasing the heat transfer rate in TFHEs. VGs are protrusions from a surface that intensify the heat transfer interrupting boundary layers, developing vortices, mixing flow and causing flow destabilization on the air side. Furthermore, this enhancement mechanism is associated with a high pressure-drop penalty. There are two types of VGs: Transverse VGs (TVG) and longitudinal VGs (LVG). TVGs develop transverse vortices (TVs) which are perpendicular to the flow direction, while LVGs generate longitudinal vortices that last over long distances in the flow channel, resulting in a more efficient heat transfer enhancement. [3][4].

The angle of attack, aspect ratio and LVG design have a significant effect on heat transfer enhancement. The delta winglet type is one of the most studied LVG given that its usage causes a lower pressure loss when compared to other vortex generators [5]. The following are effects caused by the generated LV system : the main vortex, corner vortex and an induced vortex which is the consequence of the combined effect of the aforementioned vortices, as Figure 2.2 shows [6].

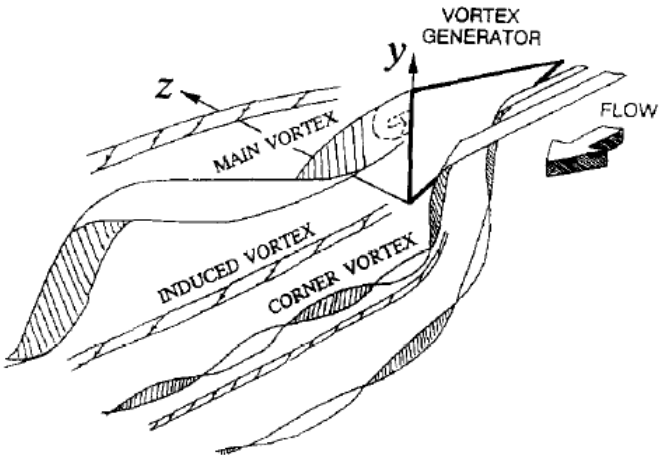

Figure 2.2: Wake structure generated by winglet [6].

2.3. Governing equations

The fluid (air) is assumed to be incompressible with constant properties. Governing equations in the computational domain can be expressed as follows:

2.3.1. Continuity Equation

$$\frac{\partial u}{\partial x} + \frac{\partial v}{\partial y} + \frac{\partial w}{\partial z} = 0 \tag{2.1}$$

2.3.2. Momentum Equation

$$\rho\left(\frac{\partial u}{\partial t} + u\frac{\partial u}{\partial x} + v\frac{\partial u}{\partial y} + w\frac{\partial u}{\partial z}\right) = -\frac{\partial p}{\partial x} + \mu\nabla^2 u \tag{2.2}$$

$$\rho\left(\frac{\partial v}{\partial t} + u\frac{\partial v}{\partial x} + v\frac{\partial v}{\partial y} + w\frac{\partial v}{\partial z}\right) = -\frac{\partial p}{\partial y} + \mu\nabla^2 v \tag{2.3}$$

$$\rho\left(\frac{\partial w}{\partial t} + u\frac{\partial w}{\partial x} + v\frac{\partial w}{\partial y} + w\frac{\partial w}{\partial z}\right) = -\frac{\partial p}{\partial z} + \mu\nabla^2 w \tag{2.4}$$

2.3.3. Energy Equation

$$\rho C_p\left(\frac{\partial T}{\partial t} + u\frac{\partial T}{\partial x} + v\frac{\partial T}{\partial y} + w\frac{\partial T}{\partial z}\right) = k\nabla^2 T \tag{2.5}$$

2.4. Previous Research

In the hopes of finding a significant improvement in performance, several studies have examined the flow structure and heat transfer characteristics for TFHEs. Researchers have attempted to evaluate the impact of passive techniques (without any external power) on the air-side of the HE as the implementation of VGs and variation of different tube parameters.

During decades the LVG implementation for passive heat transfer enhancement has been widely studied. In 1998, Fiebig [3] published "Vortices, generators and heat transfer" where he identified connections between previous studies on TV and LV systems and their application in heat transfer. The author concluded that LVs improve the heat transfer performance locally and globally in laminar and turbulent flow and they are more efficient than TVs. Fiebig also compared two types of vortex generators: wing and winglet. Using the same parameters, he discovered that heat transfer was greatly enhanced by winglet VGs in laminar regimen with low Reynolds. The author's publication served as a starting point for future research on CHEs.

Another passive technique proposed by Fiebig et al [7] provided an experimental analysis of the effect of in-line and staggered tube rows. The researchers suggested a link between heat transfer enhancement and staggered tubes, which included an increase of pressure loss. These occurrences can be explained through the emergence of a stronger horseshoe vortex after each row of tubes which affects the flow structure over a larger fin area. The effect of the staggered tubes can be seen in Figure 2.3.

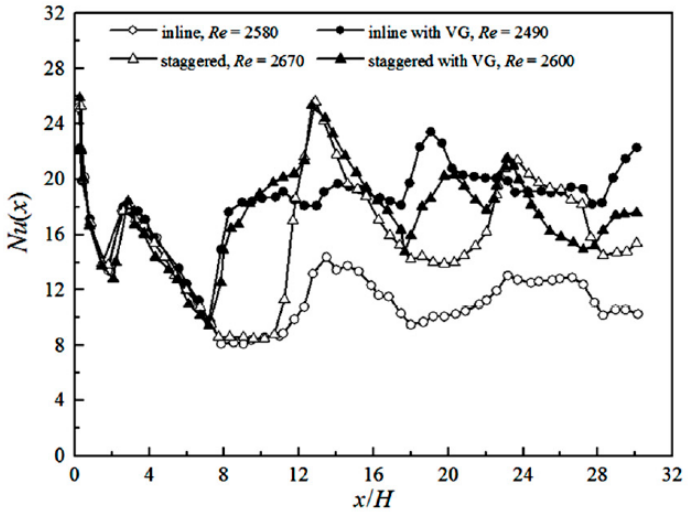

Figure 2.3: Span-average Nusselt for different arrangements [7].

This study was supported by an experimental analysis conducted by Kwak et al [8] (2002) who complemented Fiebig et al's [7] research by varying the number of tube rows. They realized that an increase in tube rows leads to a gradual improvement of heat transfer with an increase of the Reynolds number because of a larger area. Moreover, the study also compared the performance of in-line and staggered tubes, concluding that although staggered tubes show a higher heat transfer, in-line tubes arrangements have a better performance because there is less pressure loss, as seen in Figure 2.4.

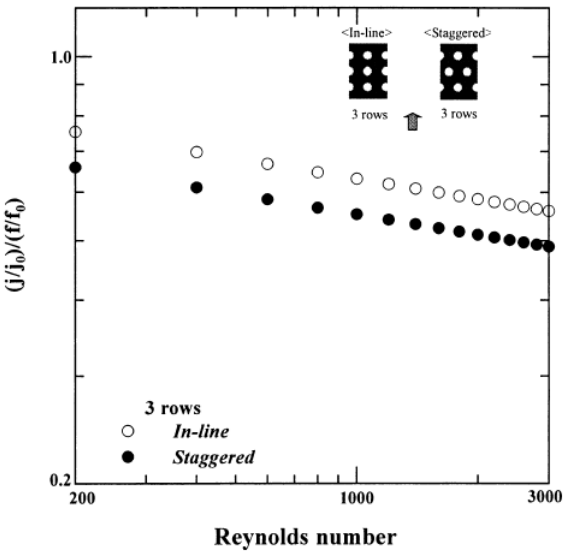

Figure 2.4: Performance comparison between in-line and staggered arrangements [8].

Torii and Kwak et al [9][10][11] also studied the effect of DWVGs in staggered and in-line circular tubes arrangement. Their study focused on the impact of delta winglets in heat transfer and pressure loss. In their research, they proposed built-in vortex generators with a CFD arrangement initially only in the first row and then in the first two rows of tubes. Compared to the CFU VG configuration from Fiebig et al [7], their experimental results showed an augmentation of heat transfer and pressure loss from 6% to 15% and 61% to 117%, respectively for the model with VGs in the first two rows.

Changing the shape of the tubes is another passive technique. Fiebig et al [12] conducted an experimental study where the local heat transfer of flat and circular staggered tubes was measured for Reynolds between 600 and 3000. They also investigated the influence of LVG and found that flat tubes presented a better heat transfer performance than circular tubes. Another finding was that the local Nusselt number increases dramatically in the case of flat tubes because of a larger influence area. However, circular tubes are more common in HEs.

Another tube shape consists of an oval type for compact TFHE. Han et al [13] examined oval and different circular tubes for finned heat exchangers through numerical research. In addition, they applied another passive technique consisting of two types of enhanced fins: louvered and wavy fin. They concluded that the oval geometry improved the flow characteristics in the wake region. This configuration reduces the flow resistance, achieving a uniform temperature distribution in the fin. Figure 2.5 shows the area goodness factor j/f (a performance factor) for the different tube shapes and fin types.

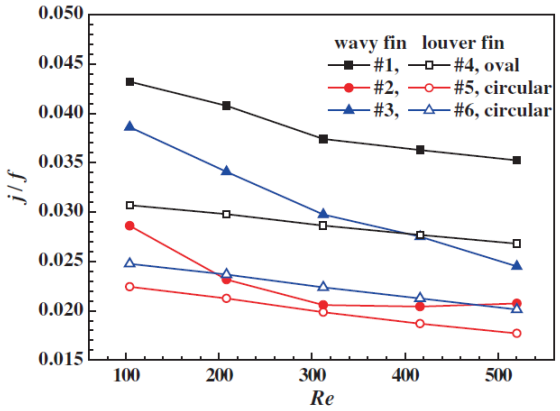

Figure 2.5: Performance comparison [13].

Similarly, a number of studies have described a connection between the shape and geometric parameters of VGs and heat transfer enhancement. In fact, this connection was confirmed by Gentry et al. [14] who suggested a direct dependency between the vortex strength and the Reynolds number, wing aspect ratio and wing angle of attack. Moreover, Diaz et al. [15] reviewed previous studies that analyzed the impact of tube and VG shapes. In their research, they performed a numerical analysis to study heat transfer and pressure loss in oval tube CHEs with laminar flow. They compared the influence of different types of LVGs proposed by previous studies: delta-type, rectangular, elliptical and spoon-type. Even though all of the VG types improved heat transfer, the delta winglet type showed the highest increase.

A number of studies has suggested that the influence of VG geometric parameters on the heat transfer and flow characteristics is correlated to the type of tube, its arrangement and VG type, in other words, the HE's configuration. For example, Wu et al [16] experimentally and numerically studied the effects of the angle of attack of the DWVG for a CHE without tubes. In their research, they concluded that 45 degrees is the best angle in terms of Nusselt number and friction factor results. Likewise, in an in-line circular tube and DWVG type configuration this angle showed the highest heat transfer enhancement for low Reynolds in another Wu et al's. [17] analysis. Lei et al [18] obtained different results. They compared different angle values using Reynolds from 600 to 2600, but adding staggered circular tubes. In their study, they also analyzed the influence of the aspect ratio, which is the ratio between the base length and the height of the vortex generator. They combined these two parameters and concluded that for a two circular tube row CHE with DWVG, the best performance was achieved with an aspect ratio of 2 and an angle of attack of 20 degrees, which is different from the result obtained by Wu et al [16], [17].

As previously mentioned, oval tubes exhibited a higher increase of heat transfer than circular tubes. Due to this enhancement, this review will focus on oval tubes configuration. Chu et al [19] carried out a study similar to Lei et al's [18] but using oval tubes and various number of tubes per row (from 2 to 5) instead of only two. They applied the same principle, the field synergy principle, to provide a fundamental understanding of the heat transfer enhancement and its relation with the flow structure. Chu et al [19] obtained different results for the 2-row case. The angle of attack of 30 degrees had the best performance for oval tubes and the best average Nusselt number, which decreased for higher angles due to the combined effect of TVs and vortices breakdown. The friction factor also increased with the angle of

attack because of a larger form drag that leads to a higher pressure loss. Additionally, Chu et al. [19] state a relation between the Nusselt number and the number of tubes per row. For a higher amount of tubes, the Nusselt number and the friction factor decreased. Therefore, the fewer the tubes per row, the better the performance. For practical applications, however, they suggested using 2 or 3 tubes per row for a better analysis.

The amount of LVGs in the flow channel also impacts the flow characteristics and heat transfer. He et al [20] conducted a study on the effect of the array of DWVGs. They proposed three different configurations: one large winglet and two arrays of discontinuous winglets. The latter showed a better heat transfer coefficient, about 33.8-70.6%, compared to a plain fin. Tiwari et al [21] studied the impact of different configurations of DWVGs on heat transfer. In their research, they proposed various configurations of winglet pairs. The span-average Nusselt number was calculated and they concluded that the more LVGS pairs, the better the heat transfer, along with a higher pressure loss.

While some studies have focused on the amount of LVGS, others have analyzed the effect of LVG's orientation in channel flow that depends on the HE configuration. For instance, Tian et al. [22] studied the effect of one pair of DWVGs in CFU and CFD configurations in a compact heat exchanger without tubes. Their study suggested that the overall performance between CFU and CFD configuration was very similar. In fact, most published studies had utilized a downstream CFD configuration. Tian et al. [22] results can be complemented with the research from Sinha et al [23] who conducted a similar study where two pairs of VGs were used, and as Tian et al. [22], their design did not include any tubes. In this case, they proposed different configurations: CFD-CFD, CFU-CFU, CFD-CFU in-line and staggered. They concluded that the CFU-CFU placement showed the best performance in terms of heat transfer. As stated before, the effect of the orientation depends on the configuration, and the configuration of the aforementioned studies did not consider any tubes.

Chen et al [24] combined CFD and CFU delta winglet VG orientation in an upstream configuration, but this time they worked with tubes. They studied the effect of these arrangements in a fin and oval tube CHE with an aspect ratio of 2, angle of attack of 30 degrees and a fixed Reynolds number of 300. The staggered configuration showed a notorious impact in the LV which lasted longer and was stronger. In contrast with Tian et al. [22], the combination of CFU and CFD showed a better performance. Such combinations improved heat transfer enhancement regardless of their sequence. It is important to notice that Chen et al [24] applied an upstream configuration of the LVGS, but most of the research considers a downstream orientation. Pesteei et al. [25] conducted an experimental study on the effects of one pair of the DWVGs location in the flow channel with a fixed Reynolds number of 2250. They concluded that the heat transfer enhancement was more effective when the VGs were positioned downstream.

These studies presented numerous HE configurations, each one with their own detailed parameters and arrangements. Hence, the studies themselves cannot be compared. Instead of establishing comparisons, researchers have managed to compile, over the years, large numbers of CHEs studies[3], [5], [26], [27]. They have helped to identify which configurations and parameters display an improved heat transfer enhancement. The purpose of this research is to quantify the enhancement between the proposed designs that showed a superior performance.

Chapter 3

Solution Method

For the numerical analysis of heat transfer enhancement in FTHE with LVG the listed steps were followed:

1. **Literature Review**: To ensure a correct comprehension of the phenomena involved and be able to recognize boundary conditions and parameters for this study. This step also helped to have a clear idea of the state of the art of heat transfer enhancement using LVGs.
2. **Design of Physical Models**: For the validation and proposed designs.
3. **Model validation and grid independence**: To describe the numerical method utilized and comparing results with Lei et al's [18] research.
4. **Numerical Simulations**: Where the software Ansys Fluent 18.2 was used and the numerical method from the validation was applied.
5. **Discussions and conclusions**: Finally, the results obtained were analyzed, the phenomena involved and flow behaviour were described and a superior performance design was found by comparing factors of interest.

3.1. Physical Model

3.1.1. Validation Model

To validate the present work, Lei et al [18] study was replicated. Their geometry aids the present work because it presents relevant geometric configurations required for this particular study, as the use of DWVG and staggered circular tubes, as shown in Figure 3.1. The proposed TFHEs's designs in this study were based on the validation geometry, its dimensions are shown in Table 3.1.

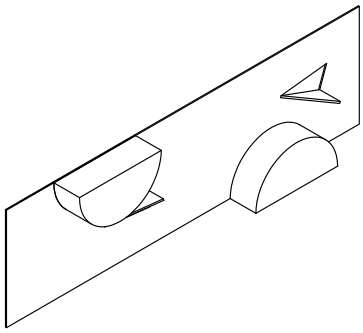

Figure 3.1: TFHE's design proposed by Lei et al [18].

Table 3.1: Lei et al [18] TFHE's geometric details.

Dimension	**Value**
Transverse pitch (T_p) [mm]	12.7
Longitudinal pitch (L_p) [mm]	22
Fin pitch (F_p) [mm]	3.2
Fin thickness (F_t) [mm]	0.13
Fin collar outside diameter (D) [mm]	10.23
Air flow direction length (L) [mm]	44
DWLVG angle of attack [°]	20
Aspect ratio	2

3.1.2. TFHE's Designs

In this study, six TFHEs designs were proposed in base of previous studies reviewed in Section 2.4. These geometries were generated using Inventor Professional Autodesk. Every case is more complex than its precursor, starting with a plane fin without DWLVG. The geometric parameters of the proposed TFHEs are near-identical to the parameters of the validation TFHE. The new dimensions are displayed in Figure 3.2 and are listed as follows:

Table 3.2: Proposed geometric details for TFHEs.

Dimension	**Value**
Fin collar outside diameter, circular tube case (D) [mm]	10.207
Air flow direction length (L) [mm]	70
DWLVG angle of attack [°]	30

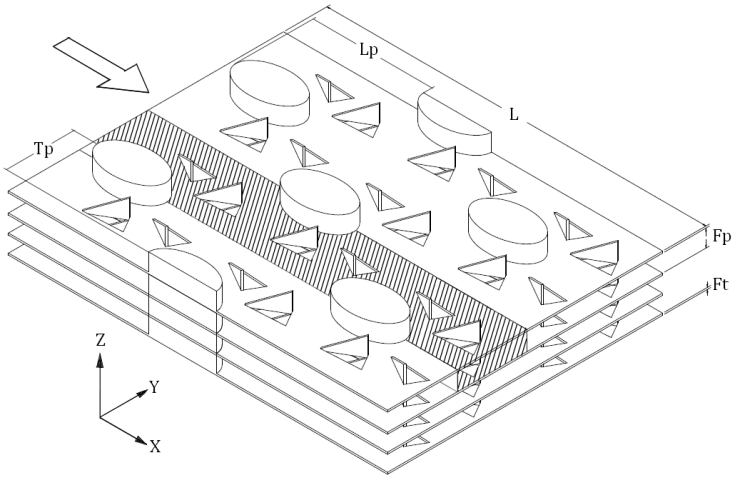

Figure 3.2: TFHE's design.

- Case 0: In-line circular tubes and no LVG (Figure 3.3 (a), base case)
- Case 1: Staggered circular tubes and no LVG (Figure 3.3 (b)).
- Case 2: Staggered oval tubes and no LVG (Figure 3.3 (c)).
- Case 3: Staggered oval tubes with one pair of DWLVG per tube in CFD orientation (Figure 3.3(d)).
- Case 4: Staggered oval tubes with two pairs of DWLVG per tube in CFD-CFD orientation (Figure 3.3 (e)).
- Case 5: Staggered oval tubes with two pairs of DWLVG per tube in CFU-CFD orientation (Figure 3.3 (f)).

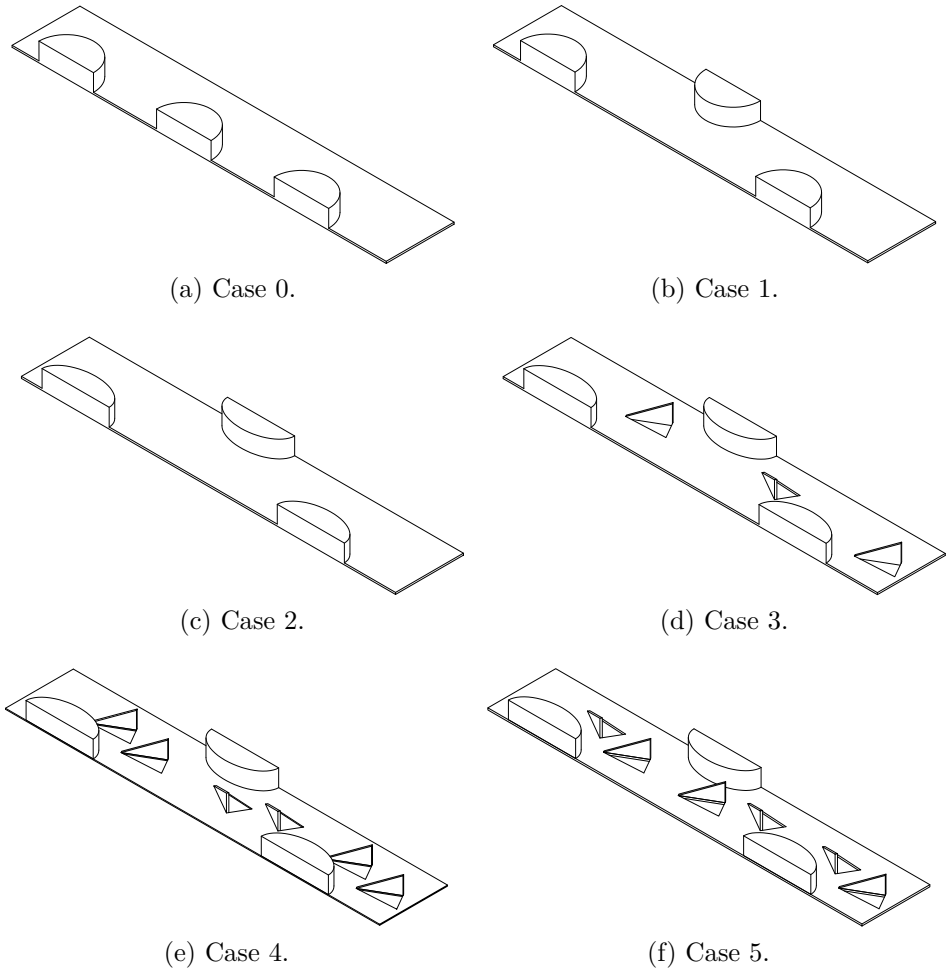

(a) Case 0. (b) Case 1.

(c) Case 2. (d) Case 3.

(e) Case 4. (f) Case 5.

Figure 3.3: TFHEs's designs.

The dimensions of the oval tubes were calculated based on the perimeter of the circular tubes (diameter: 10,207 mm), so the same heat transfer area was considered. In case 5, the second DWLVG has the same parameters as the second DWLVG in Case 4. Specific geometric dimensions in millimeters are shown in Figures 3.4 and 3.5:

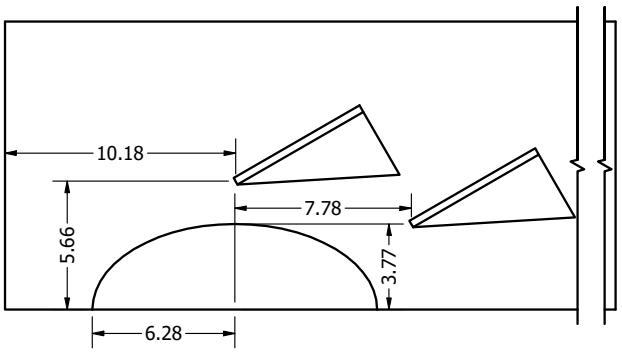

Figure 3.4: Case 4's geometric details.

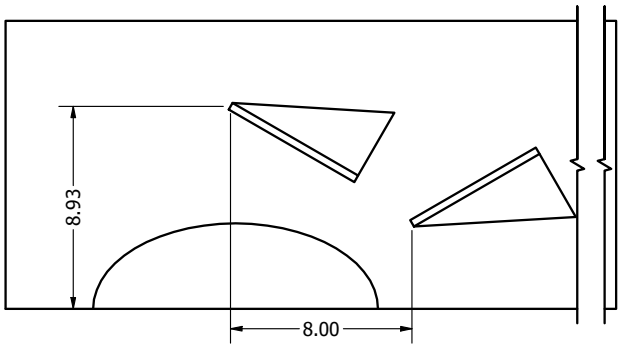

Figure 3.5: Case 5's geometric details.

3.2. Boundary conditions

The geometry was divided into three regions: Upstream-extended, fin and downstream-extended region. At the inlet boundary, u_{in} is the velocity and depends on the Reynolds number and hydraulic diameter (or tube diameter for the validation case). For upper, lower and lateral boundaries in extended regions, a symmetry condition was set. Outflow and periodic condition were applied at outlet and VG region respectively. The computational domain and boundary conditions can be seen in Figure 3.6 where the extended regions were shortened.

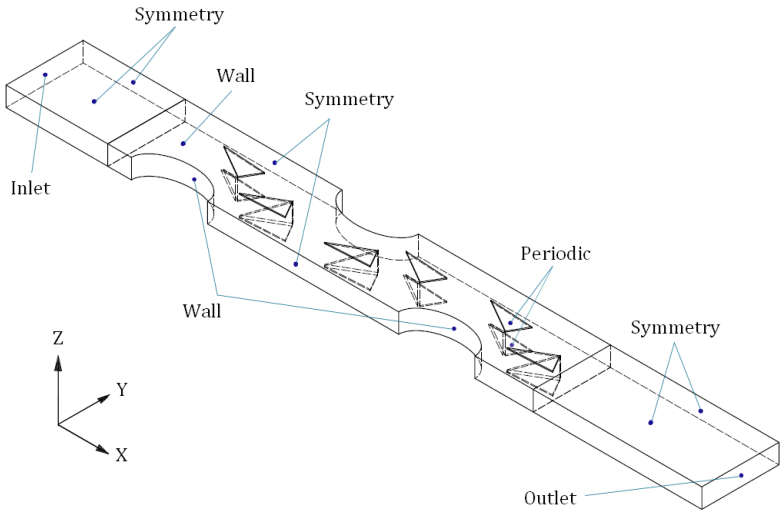

Figure 3.6: Boundary conditions on the computational domain.

3.2.1. Upstream-extended region

Inlet boundary

$$u_{in} = Constant \qquad v = w = 0 \qquad T_{in} = Constant = 293K \tag{3.1}$$

Upper and lower boundaries

$$\frac{\partial u}{\partial z} = \frac{\partial v}{\partial z} = 0 \qquad w = 0 \qquad \frac{\partial T}{\partial z} = 0 \tag{3.2}$$

Lateral boundaries

$$\frac{\partial u}{\partial y} = \frac{\partial w}{\partial y} = 0 \qquad v = 0 \qquad \frac{\partial T}{\partial y} = 0 \tag{3.3}$$

3.2.2. Downstream-extended region

Upper and lower boundaries

$$\frac{\partial u}{\partial z} = \frac{\partial v}{\partial z} = 0 \qquad w = 0 \qquad \frac{\partial T}{\partial z} = 0 \tag{3.4}$$

Lateral boundaries

$$\frac{\partial u}{\partial y} = \frac{\partial w}{\partial y} = 0 \qquad v = 0 \qquad \frac{\partial T}{\partial y} = 0 \tag{3.5}$$

Outlet boundary

$$\frac{\partial u}{\partial x} = \frac{\partial v}{\partial x} = \frac{\partial w}{\partial x} = \frac{\partial T}{\partial x} = \frac{\partial P}{\partial x} = 0 \tag{3.6}$$

3.2.3. Fin region

Fin surface and tube

$$u = v = w = 0 \qquad T_{wall} = 313K \tag{3.7}$$

Lateral boundaries

$$\frac{\partial u}{\partial y} = \frac{\partial w}{\partial y} = 0 \qquad v = 0 \qquad \frac{\partial T}{\partial y} = 0 \tag{3.8}$$

3.2.4. Parameters

Hydraulic Diameter

For non circular channels hydraulic diameter is used to calculate the Reynolds number.

$$D_h = \frac{4LA_c}{A_o} \tag{3.9}$$

Area-average pressure

Area average total pressure is calculated as it follows.

$$p_a(x) = \frac{\iint p(x,y,z)dydz}{\iint dydz} \tag{3.10}$$

Bulk Temperature

In a cross-section the bulk temperature consider the effects of the flow velocity.

$$T_{Bulk}(x) = \frac{\iint T(x,y,z) \cdot |u(x,y,z)|\, dydz}{\iint |u(x,y,z)|\, dydz} \tag{3.11}$$

Log-mean temperature difference

For obtaining the LMTD it is necessary to calculate the different temperatures at the inlet and outlet of the actual heat transfer zone using Equation 3.11.

$$LMTD = \frac{(T_{Wall} - T_{In}) - (T_{Wall} - T_{Out})}{\ln\left(\frac{T_{Wall}-T_{In}}{T_{Wall}-T_{Out}}\right)} \tag{3.12}$$

Heat transfer rate

The heat transferred per unit of time was calculated as it follows.

$$Q = \dot{m}Cp\,(T_{Out} - T_{In}) \tag{3.13}$$

Heat transfer coefficient

The heat transfer coefficient quantifies the convective heat transferred between a fluid and the wall of the HE.

$$h = \frac{Q}{A_0 LMTD} \tag{3.14}$$

Reynolds Number

The flow condition can be characterized by the Reynolds number, which can be expressed based on the fin collar diameter or the hydraulic diameter and the velocity at the minimum cross section area.

$$Re = \frac{\rho D_h U_c}{\mu} \tag{3.15}$$

$$Re = \frac{\rho D_c U_c}{\mu} \tag{3.16}$$

Nusselt Number

Dimensionless number. It's the ratio between convective and conductive heat transfer, i.e. indicates an improvement of the heat transfer of the fluid with respect to conduction, this due to the movement of the fluid.

Local Nusselt Number

$$Nu_{local}(x,z) = \left(\frac{\dot{q}(x,z)|_{y=0}}{T_{Fin}(x,z)|_{y=0} - T_{Bulk}(x)} + \frac{\dot{q}(x,z)|_{y=H}}{T_{Fin}(x,z)|_{y=H} - T_{Bulk}(x)}\right)\frac{D_h}{2k_{Air}} \tag{3.17}$$

Span average Nusselt Number

Where b(x) corresponds to the fin width.

$$Nu_{sp}(x) = \frac{1}{b(x)}\int_0^{b(x)} Nu_{local}(x,y)dy \tag{3.18}$$

Average Nusselt Number

$$Nu_a = \iint Nu(x,y)dxdy \tag{3.19}$$

$$Nu_a = \frac{hD_h}{k_{air}} \tag{3.20}$$

Friction factor

Dimensionless number, with which the pressure losses due to fluid friction are quantified.

$$f = \frac{2\Delta P}{\rho {U_c}^2}\frac{A_c}{A_0} \tag{3.21}$$

Thermal performance factor

Where Nu_0 and f_0 correspond to the average Nusselt number and the friction factor calculated for the base case (Case 0) respectively.

$$JFw = \frac{Nu/Nu_0}{(f/f_0)^{1/3}} \tag{3.22}$$

3.3. Model Validation

3.3.1. Grid generation

To mesh the geometry, it was imperative to generate the computational domain that is shown in Figure 3.6. Three parts can be distinguished: The original heat transfer zone, the extended upstream and the downstream regions. At the entrance, the region was extended until reaching the length of the heat transfer zone for flow uniformity. To ensure there was not any flow recirculation, the exit domain was also extended five times the length of the heat transfer region.

The grid was generated using two types of elements: Tetrahedrons, for the actual heat transfer region consisting of a complex geometry, and hex dominant elements for extended parts, which do not required a finer grid. To improve the quality of the mesh system, "body sizing" was applied. Smaller elements were used on the heat transfer region, and the smallest elements were inside "spheres of influence", which were centered in the VGs for a better flow behavior analysis.

The resulting grid consisted of almost 430,000 elements. To ensure an optimal mesh quality the orthogonal quality and skewness criteria were considered. The specific values will be detailed in Section 3.4. The topology of the mesh is displayed in Figure 3.7:

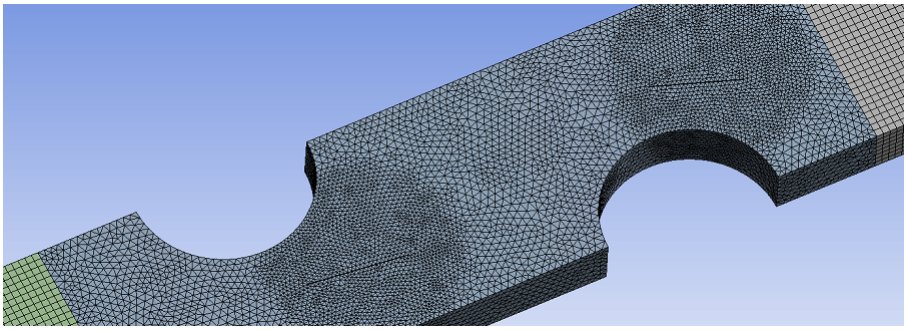

Figure 3.7: Details of the mesh.

3.3.2. Numerical method

Ansys Fluent 18.2 was used to numerically simulate the different cases, and their equations were iteratively solved using the finite volume method with SIMPLEC algorithm. As previously mentioned, the cases were based on previous studies, the flow was considered laminar and in transient condition for a correct vortex development. The time step was set in $\Delta T = 10^{-5}[s]$, and the number of time steps was selected so the simulation reached a stationary state. The convergence criterion for every time step was residuals less than 10^{-6} and 10^{-3} for energy and momentum equations.

3.3.3. Validation results

The present work was validated with the numerical results obtained by Lei et al. [18]. Their research presented important similarities with the present study: TFHE, laminar flow, the use of DWLVG and circular tubes, and well defined boundary conditions. To validate the results the geometry described in Section 3.1.1 was recreated and boundary conditions listed in Section 3.2 were applied. The software ANSYS fluent 18.2 was used to solve the simulations, fluid-solid conjugated heat transfer was modeled. The generated mesh and the numerical method employed are described in Sections 3.3.1 and 3.3.2 respectively.

To quantify the characteristic of the convective heat transferred and pressure loss the heat transfer coefficient and the friction factor values at the entrance and at the outlet were calculated. The latter for Reynolds numbers 600, 1400 and 2200. Both of them (were calculated based on area averaged temperature using Equations 3.14 and 3.21 respectively. The Reynolds number for this case was expressed as Equation 3.16.

The values obtained with the previously described methodology are shown in Figures 3.8 and 3.9. The results after the replication of Lei et al's [18] study showed the same behaviour and an error of less than 7% with the expected values, which is an acceptable error range.

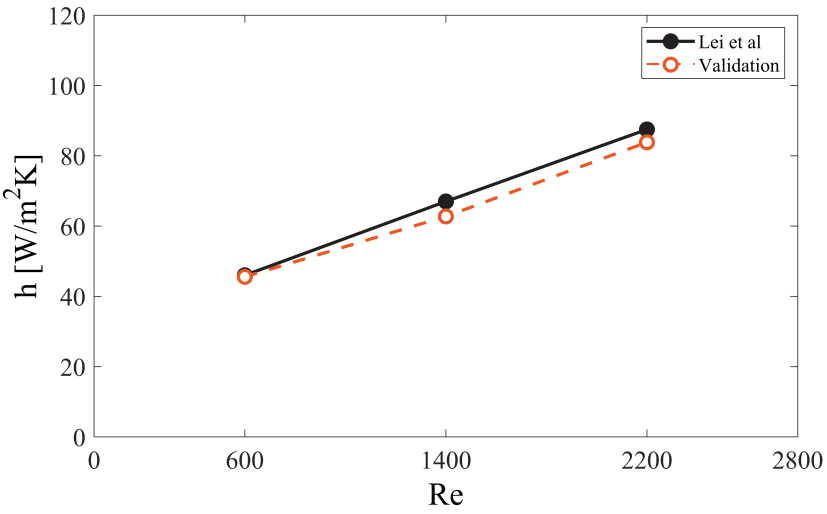

Figure 3.8: Heat transfer coefficient model validation.

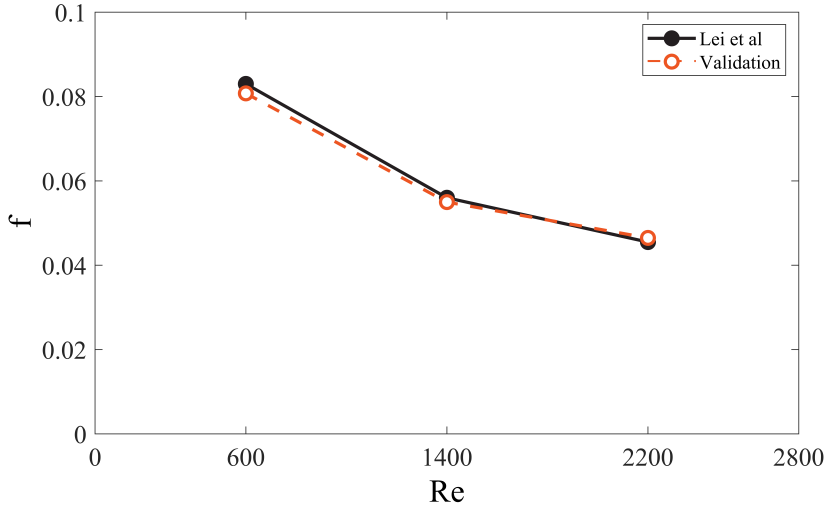

Figure 3.9: Friction factor model validation.

3.4. Grid Independence

The accuracy of a simulation depends on several factors, one of them being the element quantity and this corresponds to the mesh refinement. The amount of such elements can be increased with the type of element and body sizing in different zones. If the quantity of element changes, the result of the simulation might change. The purpose of this section is to find a number of elements with the lowest computational cost, and where the variation of results is negligible compared to finer meshes.

Three different meshes were analyzed. These grids were generated following the steps described in Section 3.3.1, their characteristics are detailed in Table 3.3. The medium mesh is the one used in the validation model, and showed little variation compared with the Lei et al's study [18]. This is why the results obtained with the other meshes were compared with the medium grid and their values showed a difference of less than 5% thus proving the grid independence. The results obtained for the different grids can be seen plotted in Figures 3.10 and 3.11.

Table 3.3: Details of the mesh

Category	Coarse Mesh	Medium Mesh	Fine Mesh
Elements	210,755	428,232	863,125
Nodes	39,883	78,826	156,567
SOI's Elements Size, mm	0.30	0.23	0.18
Max Element Size, mm	0.50	0.40	0.30

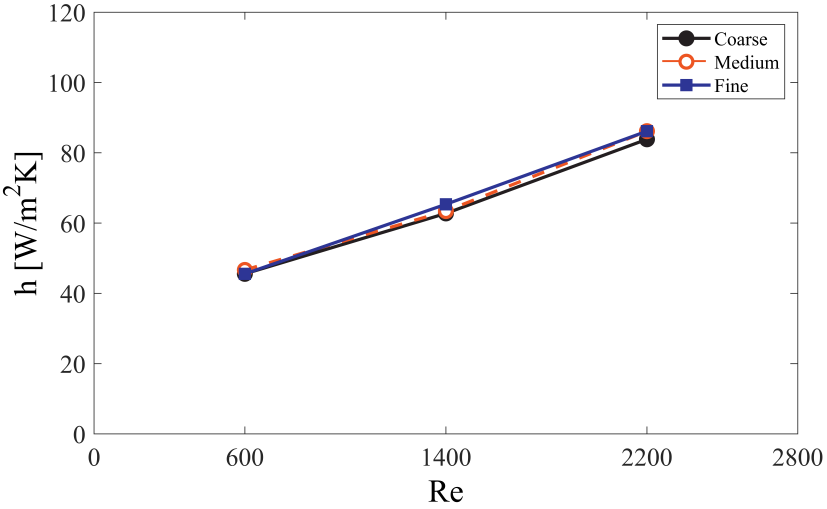

Figure 3.10: Heat transfer coefficient grid independence.

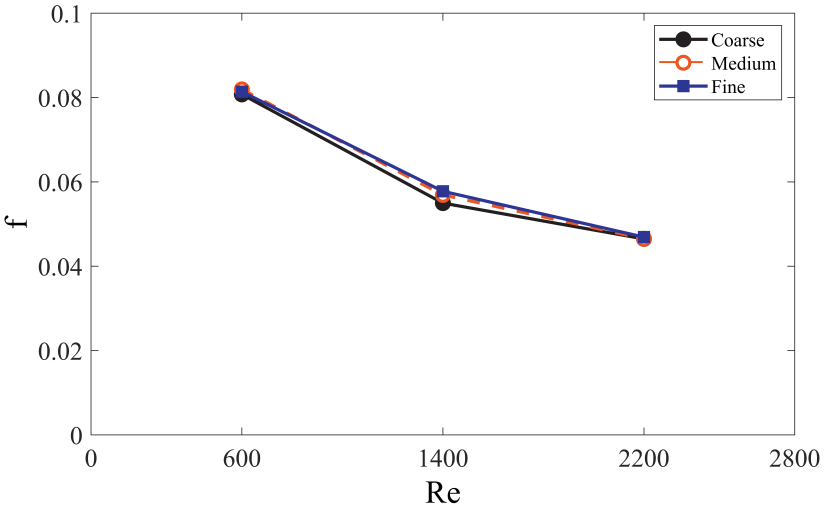

Figure 3.11: Friction factor grid independence.

Chapter 4

Results and discussion

In this section, the different results obtained will be presented and analyzed. The different contours and profiles showed in this chapter correspond to simulations with a fixed Reynolds of 2000.

4.1. Thermohydraulic behaviour

4.1.1. Case 0

A low velocity region can be recognized in Figure 4.1, caused by the recirculation in the wake behind the tubes which produces an enhancement of local temperature, as shown in Figure 4.2. This behaviour inhibits the flow mix and does not contribute to the heat transfer.

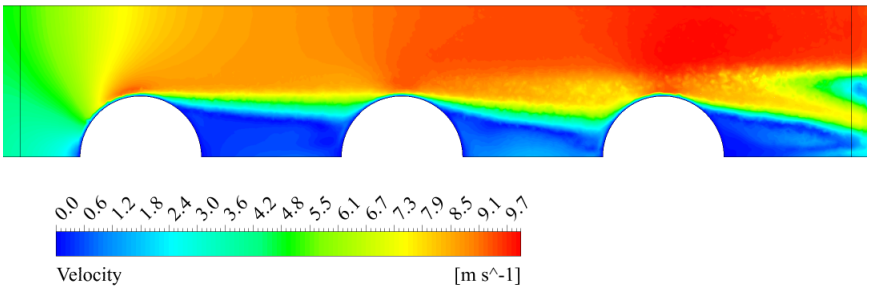

Figure 4.1: Velocity profile for Case 0.

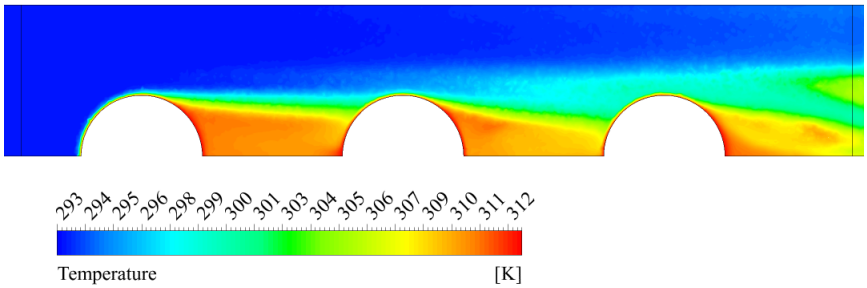

Figure 4.2: Temperature profile for Case 0.

The impact on the tubes generates turbulence, horseshoe vortices can be seen in Figure 4.3 after the tubes. The strongest vortex is caused by the third tube and the swirl leads to a heat transfer enhancement as presented in Figure 4.4 where a better flow mix is achieved.

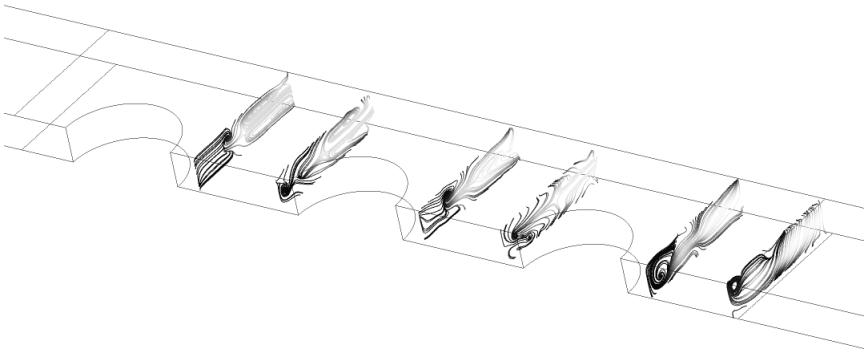

Figure 4.3: Streamlines for Case 0.

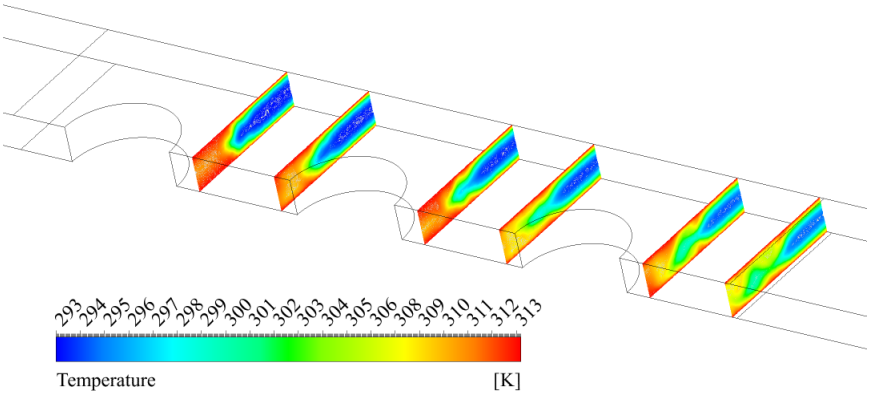

Figure 4.4: Temperature profile for Case 0.

The span average Nusselt for Case 0 is represented in Figure 4.5. The first peak appeared in front of the first tube. Then the second peak (due to the impact of the flow on the second tube) is lower than the first one because of the separation of the flow that results in a low-speed region behind the first row. The third peak is slightly higher than the second due to a stronger horseshoe vortex producing a higher speed region around the tube, which allows a better flow mix. The latter can be explained due to a smaller wake after the second tube which becomes the stagnation flow of the third row, as seen in Figure 4.1.

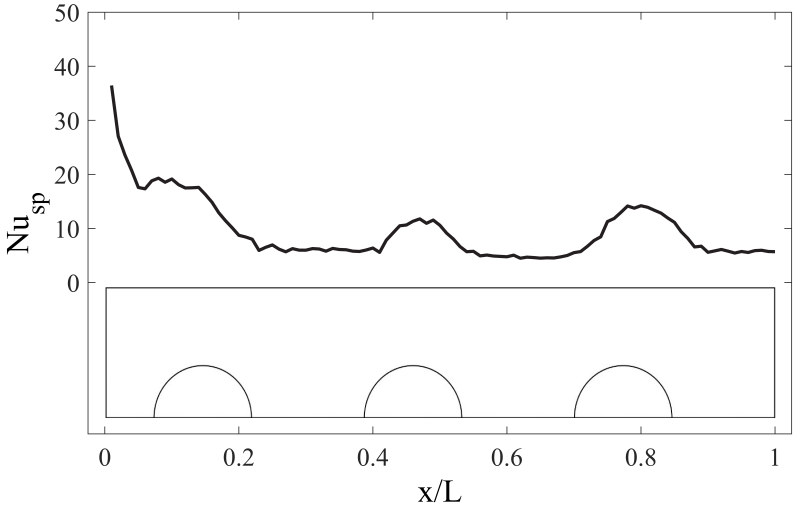

Figure 4.5: Span-average Nusselt for Case 0.

4.1.2. Case 1

Case 1 consisted of a staggered arrangement of 3 circular tubes. The span averaged Nusselt number is plotted in Figure 4.6, in this case the second peak is higher than the first one because the second tube is not longer in the first row wake region, and the low velocity region after every tube is reduced because the tubes guide the flow into the wake region of the next row as Figure 4.7 shows. This behaviour improves the flow mix even in dead water zones, and results in a better span average Nusselt number. A third peak can be recognized, caused by the impact of the flow with the third tube, which is in the wake of the first tube, and results in a lower third peak of heat transfer than the previous one.

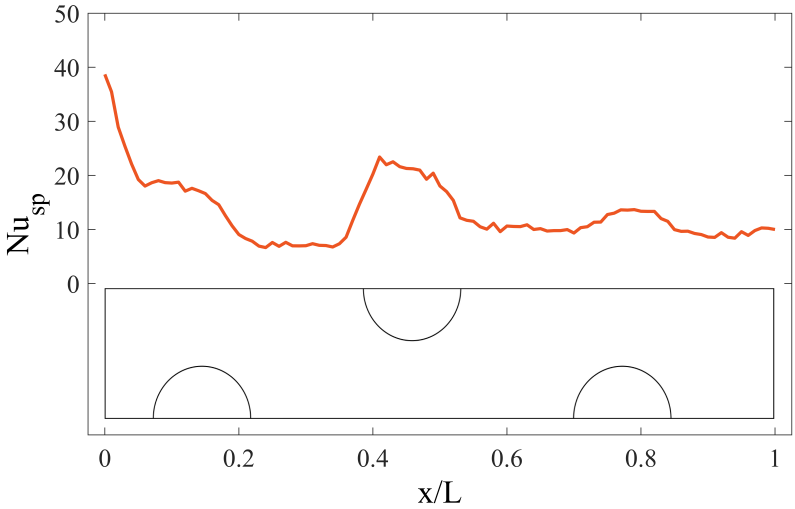

Figure 4.6: Span-average Nusselt for Case 1.

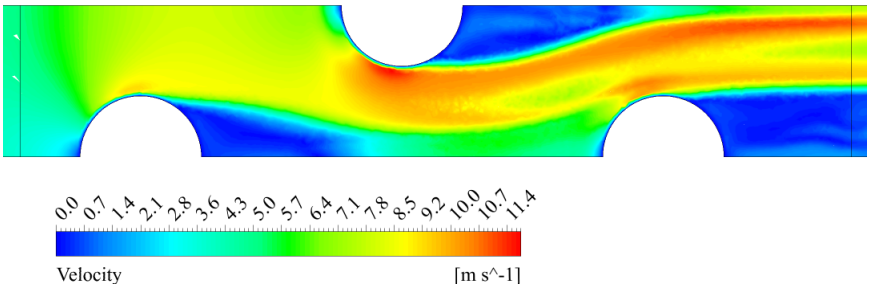

Figure 4.7: Velocity profile for Case 1.

As mentioned before, in this case there is a low velocity region behind the tubes where there is no temperature distribution, but it is smaller than the one on Case 0 because of the redirection of the flow due to the staggered arrangement, as seen in Figure 4.8.

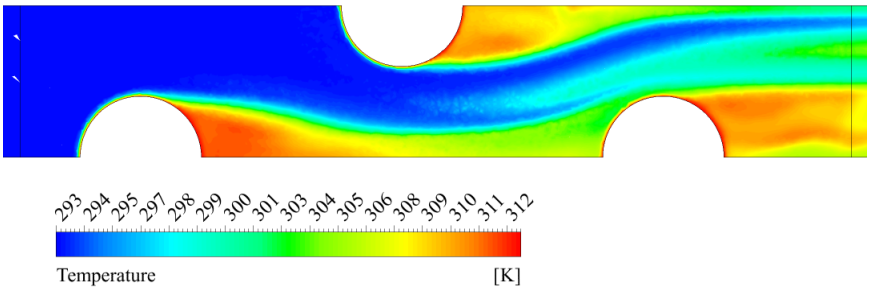

Figure 4.8: Temperature contour for Case 1.

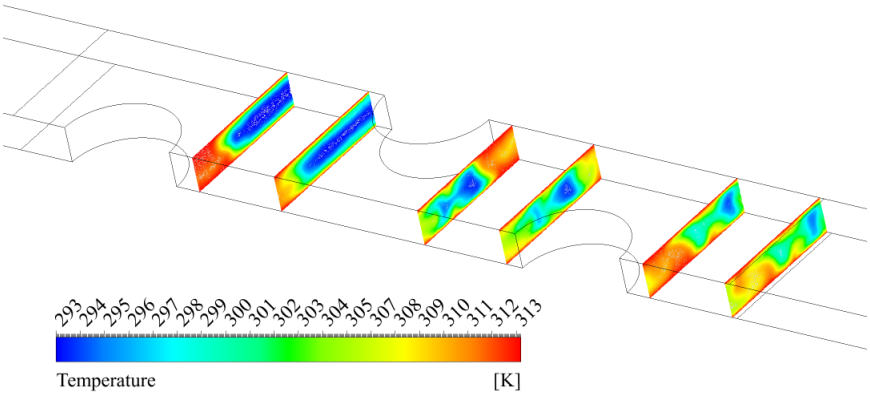

Figure 4.9: Temperature contour in different planes of Case 1.

In 4.10 the horseshoe vortices generated are illustrated, these swirls on the flow cause a perturbation on the boundary layer as seen in Figure 4.9, and because of the staggered arrangement these vortices last over longer distances than the ones in Case 0. They achieve a better temperature distribution by minimizing low velocity regions.

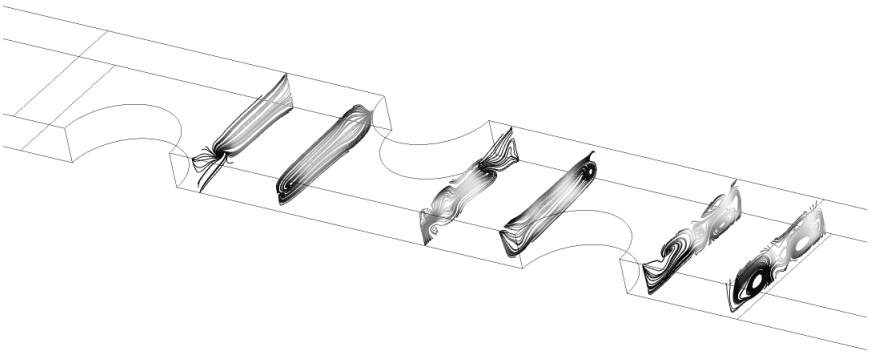

Figure 4.10: Streamlines for Case 1.

4.1.3. Case 2

This configuration is similar to Case 1, staggered tubes are used but this time with oval shape. The curve behaviour in Figure 4.11 is almost the same as Case 1. It is in the velocity profile when differences become apparent, the change of shape has an impact on the wake region making it narrower so the low velocity region is even smaller than it is in Case 1 as seen in Figure 4.12. Due to the oval shape the stagnation zone in front of every tube is smaller, and because there is a smaller wake region a better temperature distribution is achieved as Figure 4.13 illustrates.

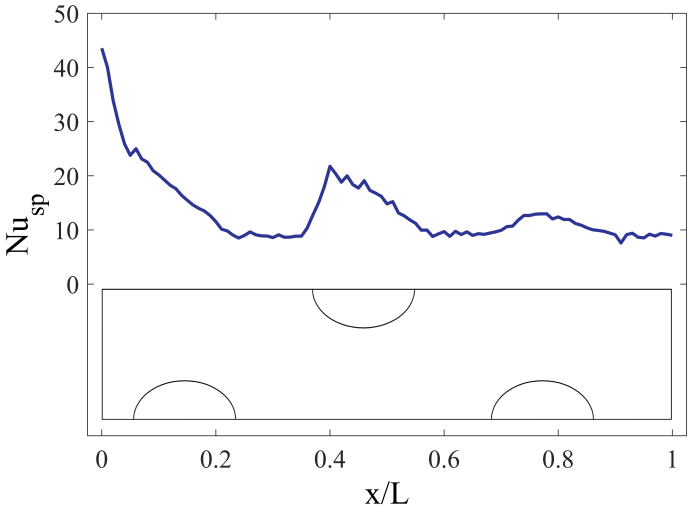

Figure 4.11: Span-average Nusselt for Case 2.

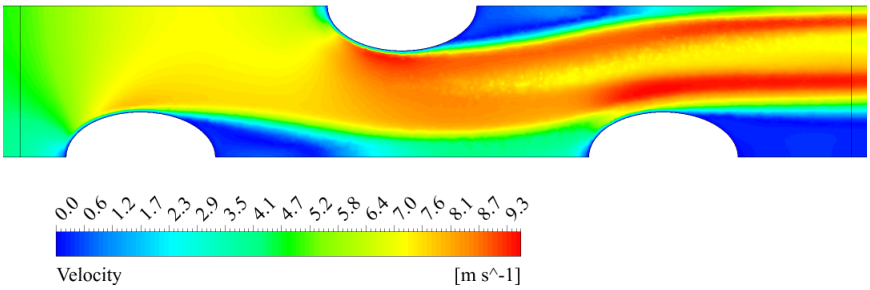

Figure 4.12: Velocity profile for Case 2.

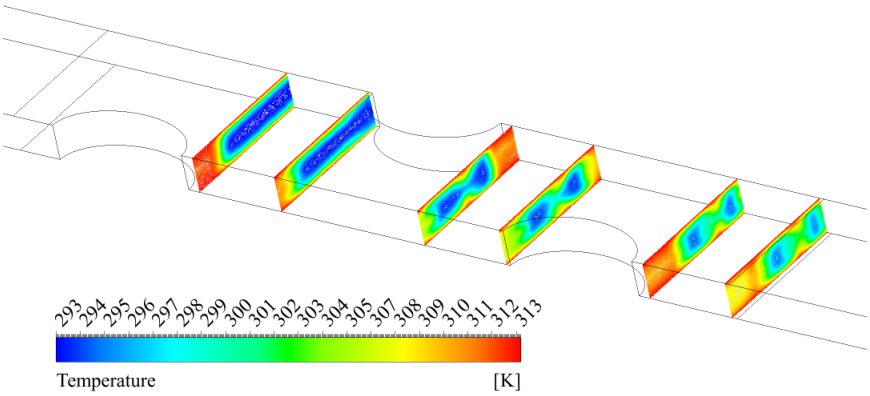

Figure 4.13: Temperature profile for Case 2.

It is important to notice that the horseshoe vortices generated in the previous case are stronger than for the present geometry. In Figure 4.14 the vortices are not as clearly defined as in Figure 4.10.

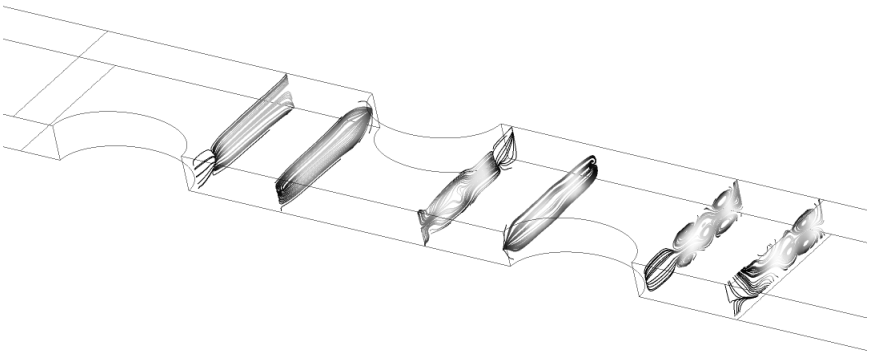

Figure 4.14: Streamlines for Case 2.

4.1.4. Case 3

Some variations can be observed on the flow behaviour in this geometry because of the addition of DWVGs. In Figure 4.15 it is possible to distinguish well defined LVs after the DWVGs, these vortices are stronger than the horseshoe vortices generated on the previous cases.

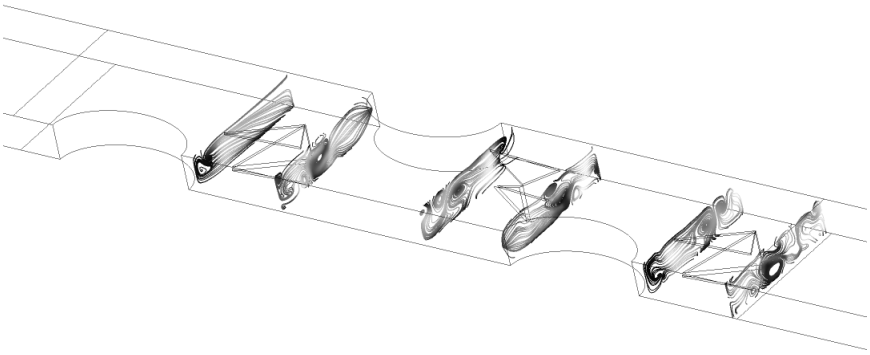

Figure 4.15: Streamlines for Case 3.

DWVGs generates LVs that destabilize the flow and improve the mix even in dead water zones. In addition, because of their downstream position there is a smaller area for the air to flow between the DWVGs and the tubes, which causes an increase in velocity as seen in Figure 4.16.

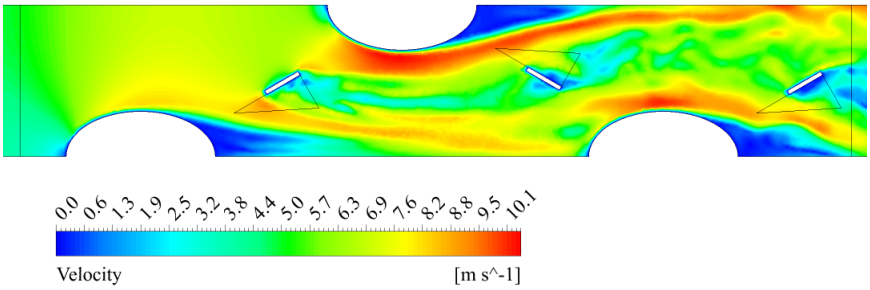

Figure 4.16: Velocity profile for Case 3.

These vortices also interrupt the development of thermal boundary layers. Their impact on the temperature distribution is shown in Figures 4.18 and 4.17, where after the DWVGs a strong and lasting LVs can be appreciated.

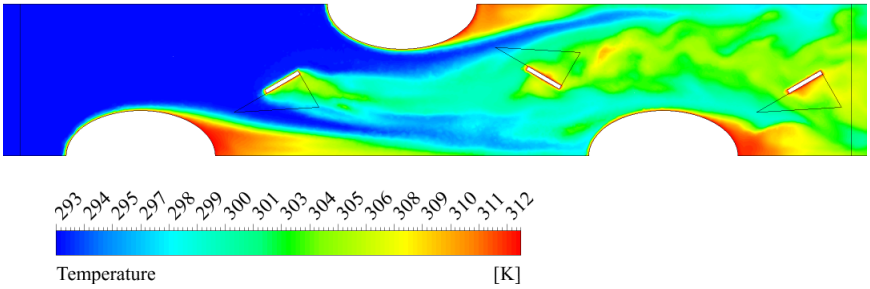

Figure 4.17: Temperature contour for Case 3.

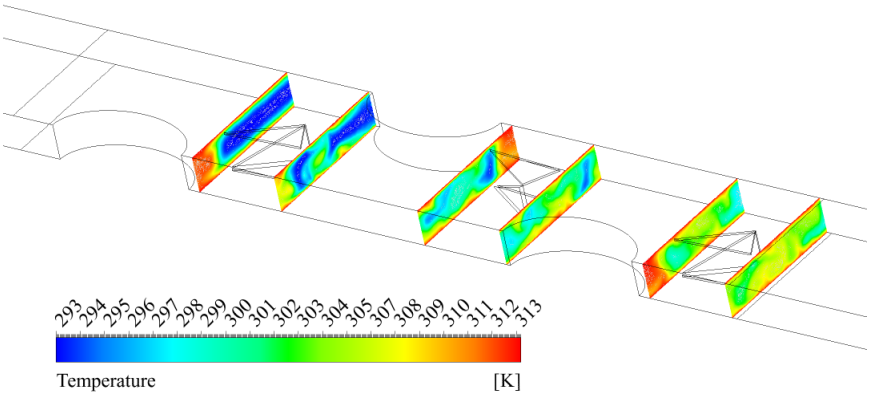

Figure 4.18: Temperature contour for Case 3.

In Figure 4.19, as expected, the behaviour of the span average Nusselt number is different than in the previous cases. Because of LVs, higher peaks are reached.

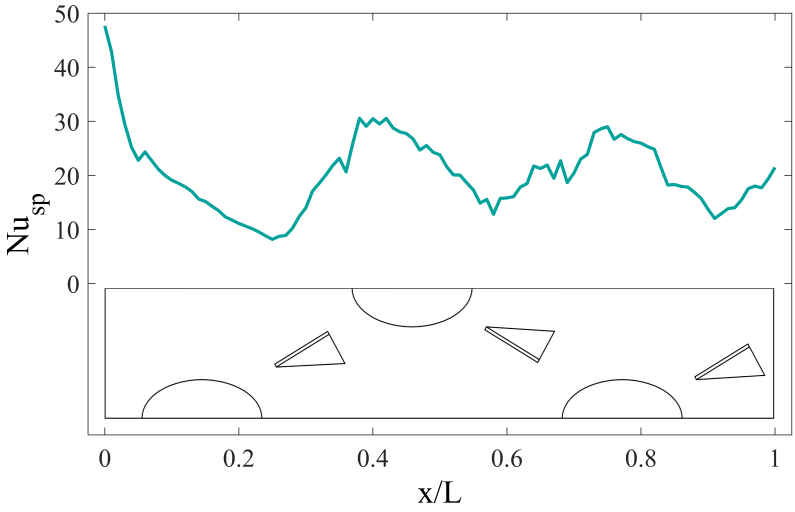

Figure 4.19: Span-average Nusselt for Case 3.

4.1.5. Case 4

As a way of improving the heat transfer rate even more, as previous studies suggested, two pairs of DWVGs with CFD-CFD orientation were applied in Case 4. The higher the number of DWVGs, the higher the flow mix, and that leads to a better temperature distribution on the channel, as Figures 4.20 and 4.21 show. It is important to notice that, due to the generated LVs the flow mix starts earlier on the channel, and their effect causes a thinner thermal boundary layer after the third tube.

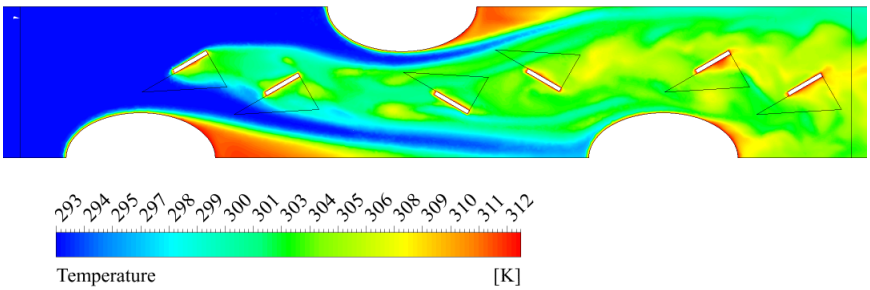

Figure 4.20: Temperature contour for Case 4.

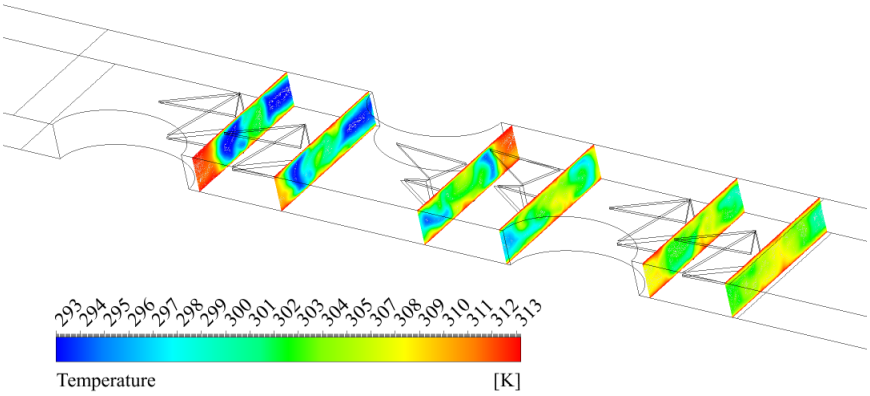

Figure 4.21: Temperature contour for Case 4.

In the same way, due to the presence of DVWGs, the air flowing near the tubes is accelerated and even higher velocity regions than the ones in Figure 4.16 (Case 3) can be observed in Figure 4.22.

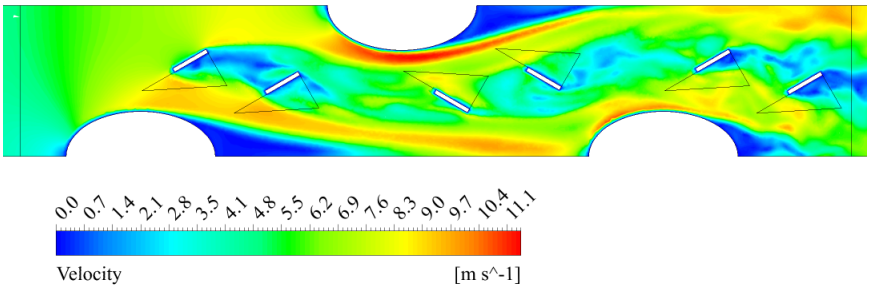

Figure 4.22: Velocity profile for Case 4.

In Figure 4.23 LVs appear after every DWVG, and also after the third tube a horseshoe vortex is generated and there is not a recirculation zone.

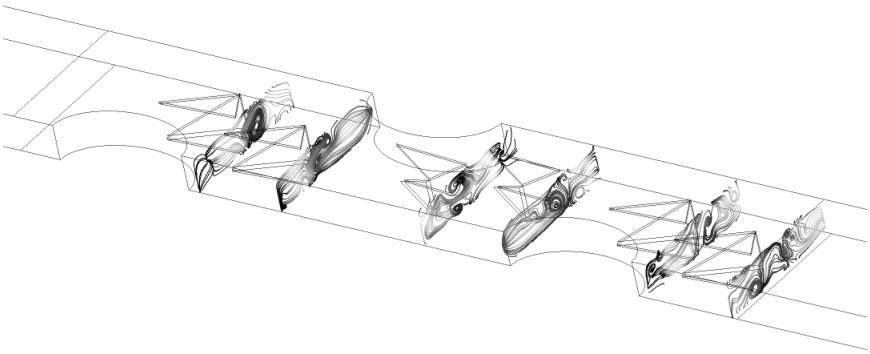

Figure 4.23: Streamlines for Case 4.

As mentioned before, one of the LVs characteristics is that they last long distances. This, combined with the highest velocity regions is translated into a better heat transfer. As contemplated and due to the different LVs effects, the highest peak is the third one as shown in Figure 4.24.

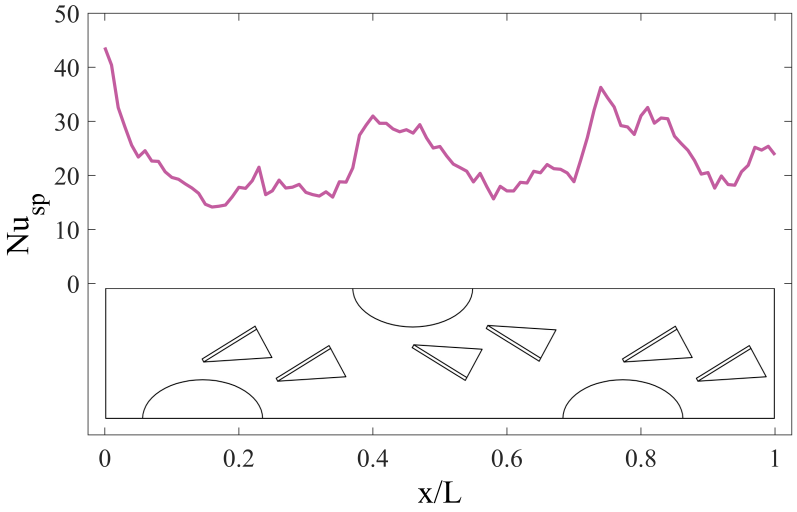

Figure 4.24: Span-average Nusselt for Case 4.

4.1.6. Case 5

After a careful literature review, to enhance heat transfer a CFU-CFD DWVG orientation was proposed. In this case the first DWVG (CFU) guides the flow to the next VG (CFD), resulting in a stronger LV as seen in Figure 4.25.

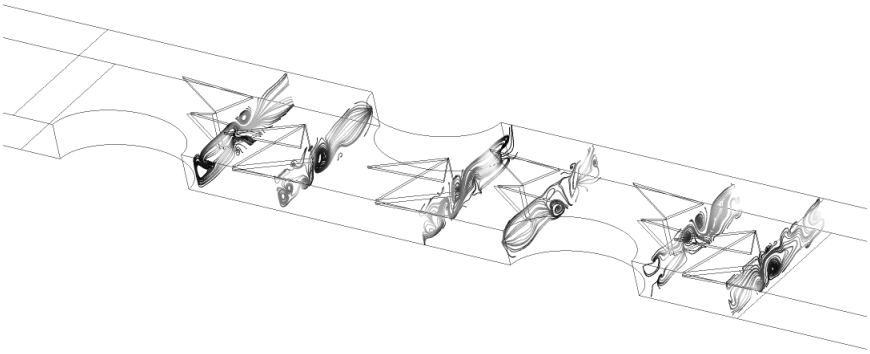

Figure 4.25: Streamlines for Case 5.

High velocity regions can also be spotted in Figure 4.26 but the ones in Case 5 reached higher velocities because the "channel" between the tubes and the DWVGs is larger in the previous case thanks to the orientation of the DWVGs.

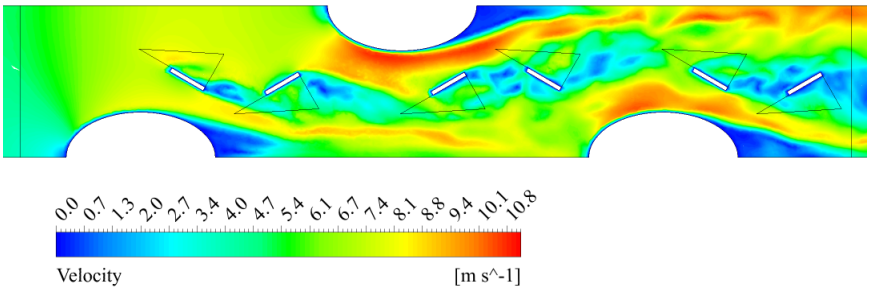

Figure 4.26: Velocity profile for Case 5.

Unlike the previous case, every thermal boundary layer development is interrupted after the tubes by the effect of the LVs as Figure 4.27 shows which results in a better temperature distribution.

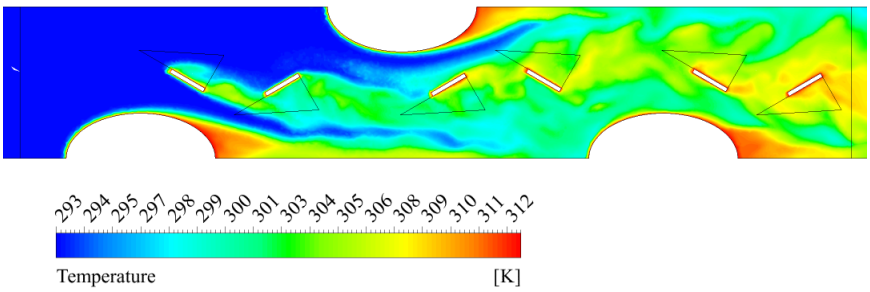

Figure 4.27: Temperature contour for Case 5.

The span average Nusselt curve plotted in Figure 4.28 has nearly the same behaviour than the curve in Case 4. In this case the third peak is lower than the second, because with the new DWVG arrangement the second VG enhances the strength of the previously generated vortex, so the heat transfer enhancement is produced in all the flow channels, and it is not focused on the third tube row as in Case 4.

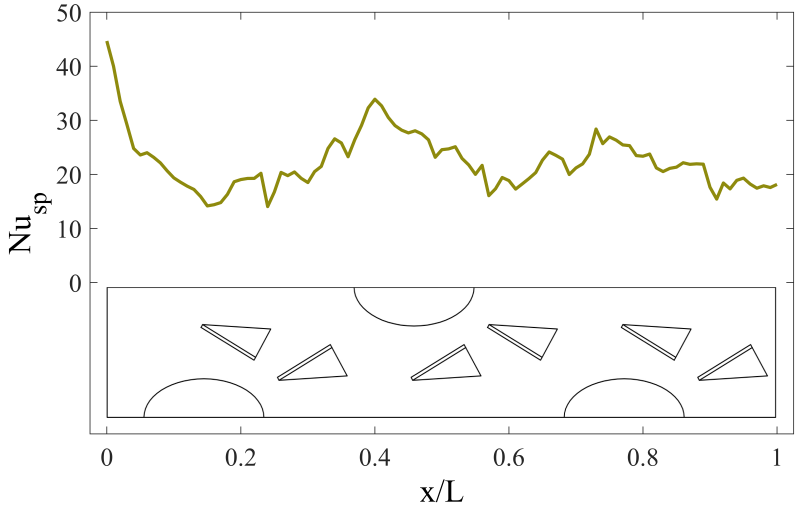

Figure 4.28: Span-average Nusselt for Case 5.

Before discussing this study's results, the effect of adding more tubes to the exchanger as a means of obtaining an optimal analysis was assessed. Figure 4.29 displays a less pronounced slope in the bulk temperature curve as the channel progresses. If such channel were longer and had more tubes, the curve would stagnate. This is also suggested by 4.30 where it can be observed that wall heat flux decreases due to the slight temperature difference between the fluid and the exchanger's walls.

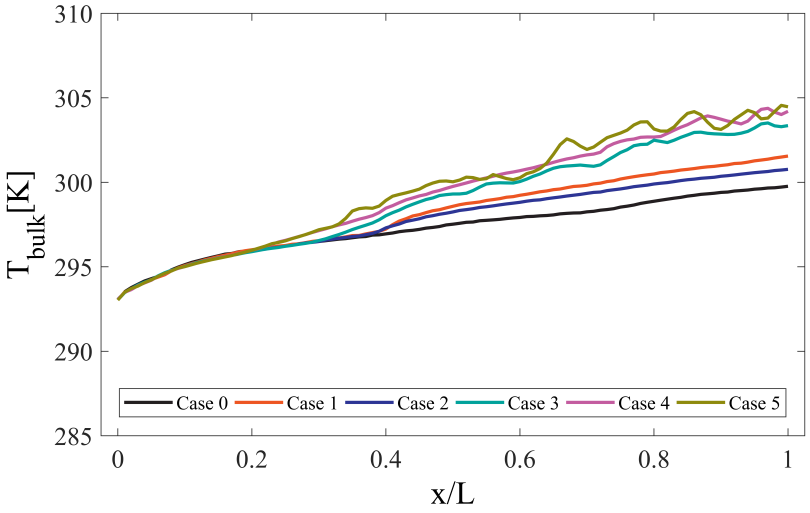

Figure 4.29: Bulk temperature in the channel.

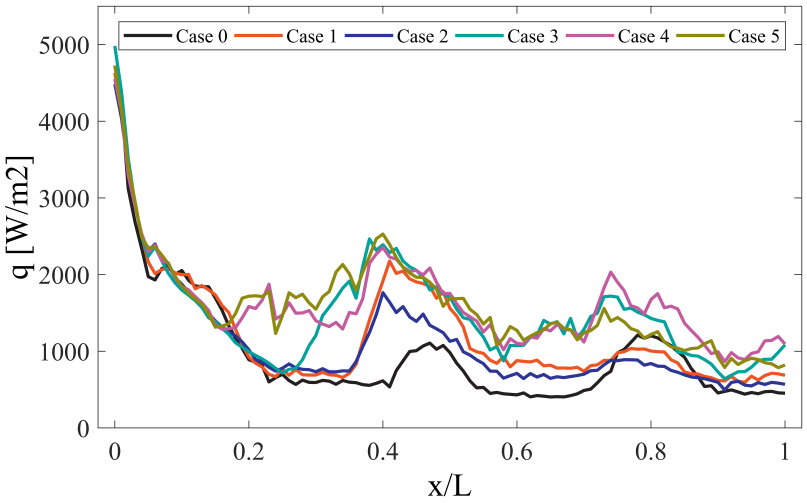

Figure 4.30: Wall heat flux in the channel.

4.2. Cases comparisons

The different cases were compared based on the span average Number for Reynolds 2000, average Nusselt, friction factor and JFw.

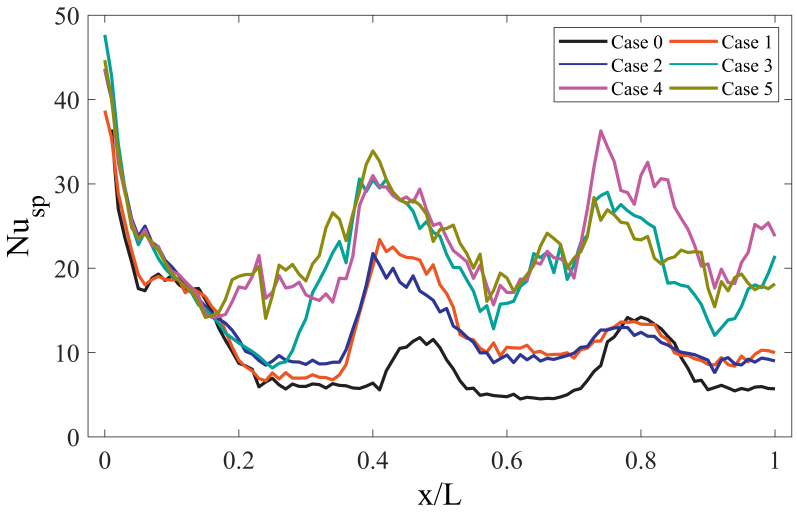

Figure 4.31: Span-average Nusselt number for Reynolds 2000

The span average Nusselt number is plotted in Figure 4.31. The staggered arrangement (Case 1, 2, 3, 4 and 5) clearly shows a better performance because the second tube in staggered arrangement guides the flow to the wake of the preceding tube. The first peak shows a quite similar behaviour depending on the shape of the tube. Smaller stagnation zones appear in front of the oval tubes and they generate a better flow mix. This is why the designs with oval tubes showed a higher first peak. The second peak begins as a consequence of the flow impact with the tube (for the cases without VGs). The curve in Case 2 reaches a lower second peak when compared to Case 1, but in Figure 4.32 the average Nusselt number

is higher for Case 2. This implies that the heat transfer enhancement achieved thanks to the smaller stagnation zone of the first tube is greater than the increase in heat transfer caused by the horseshoe vortices generated by the second tube (which are stronger for the circular tube shape design). The presence of DWVGs improves the span average Nusselt number and, in turn, the produced LVs enhance the flow mix between tubes. Thus proving that the second peak in Case 3 is higher and also wider than in the previous cases. In Figure 4.32 the average Nusselt number for different Reynolds is very similar for Cases 4 and 5, but if the span average Nusselt numbers are compared, their patterns are not the same. Global heat transfer enhancement is affected in a similar way by the strength of the vortices generated by CFU-CFD DWVGs (Case 5) and the number of vortices produced by CFD-CFD DWVGs (Case 4).

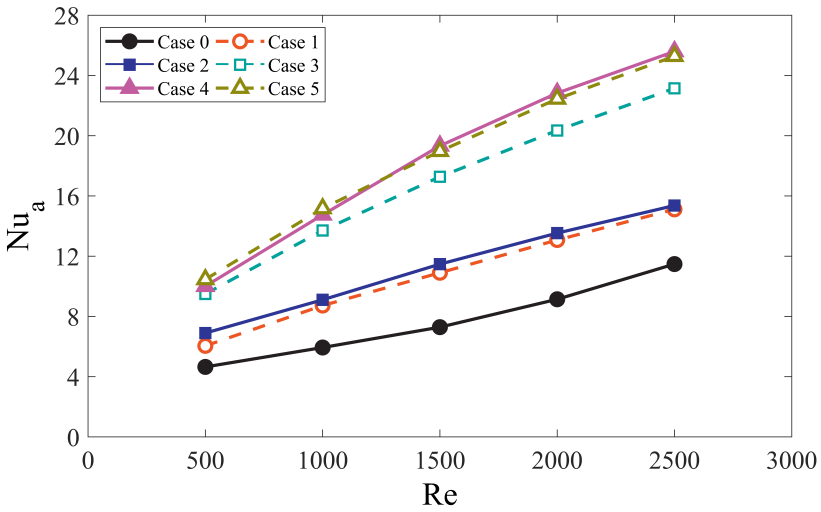

Figure 4.32: Average Nusselt number

The average Nusselt number is plotted in Figure 4.32 and it was calculated based on the span average Nusselt number (Equation 3.19). As expected, the Nusselt value increases with the Reynolds due to higher velocities, stronger vortices and better flow mix. For higher Reynolds the addition of a second pair of DWVGs produces a better heat transfer enhancement than for lower Reynolds, improving the Nusselt number by up to 30% compared with the one-pair DVWGs design.

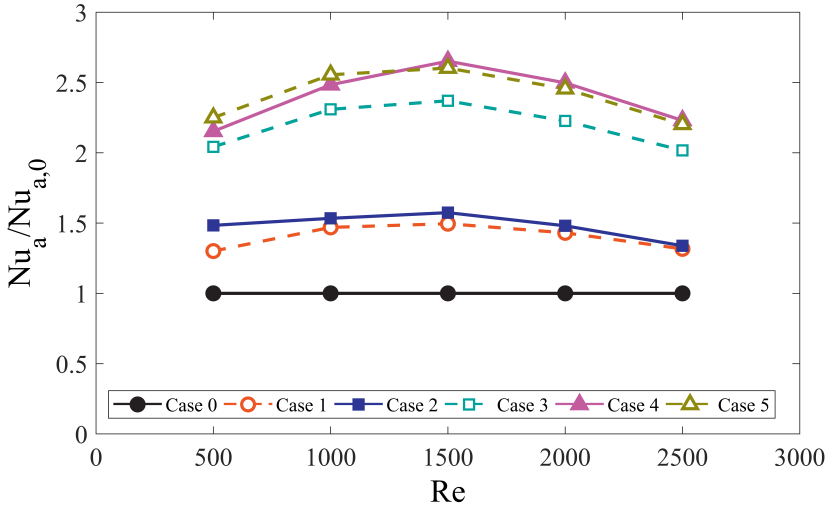

Figure 4.33: Ratio between different average Nusselt numbers and Case 0 Nusselt.

Every design was compared with the base case (Case 0) in Figure 4.33. The highest increase appears for Reynolds 1500 and Case 4 with an average Nusselt number 2.6 times bigger than the base case. The influence of DWVGs is clear, the major increase of heat transfer occurs by adding DWVGs, the Nusselt number in Case 3 for Reynolds 1500 is 50% higher than the one without VGs (Case 2). Oval tubes showed a better Nusselt ratio for lower Reynolds than circular tubes, and for higher inlet velocities their values almost converge to an identical value. The heat transfer enhancement improves with the Reynolds number augmentation for all the different cases for which Reynolds is lower than 1500. This behaviour was expected since the passive techniques applied to enhance the heat transfer showed better results for lower Reynolds in previous studies. In fact, that is the reason why the present work focused on low Reynolds.

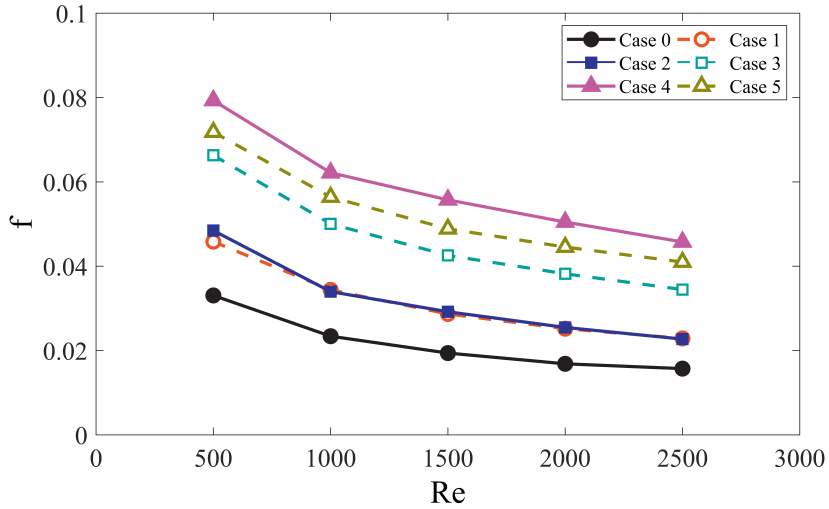

Figure 4.34: Friction factor.

The friction factor is presented in Figure 4.34. The higher the inlet velocity, the lower the friction factor. The in-line tube without DWVGs exhibits the lowest friction factor among all the cases. There is only a slight difference between Case 1 and Case 2 in terms of f since both of them feature the same pattern and values. The highest difference is about 5% for Reynolds 500. The augmentation of f in cases 3, 4 and 5 can be explained through the addition of DWVGs; the LVs generated produced a raise in the pressure loss on the channel. The higher the number of DWVGs pairs, the greater the pressure loss. VGs orientation has an important effect on pressure loss, leading to an increment from 10% to 14% on the friction factor of the CFD-CFD configuration compared to CFU-CFD arrangement. Figure 4.35 displays the friction factors for all of the cases and the pressure loss for the base case. For Reynolds lower than 2000, there is a major pressure loss as the Reynolds number increases. And the highest friction factor increase is about 2.64 times greater than the base case for Reynolds 2000 and a staggered oval tube arrangement with DWVGs in CFD-CFD orientation (Case 4).

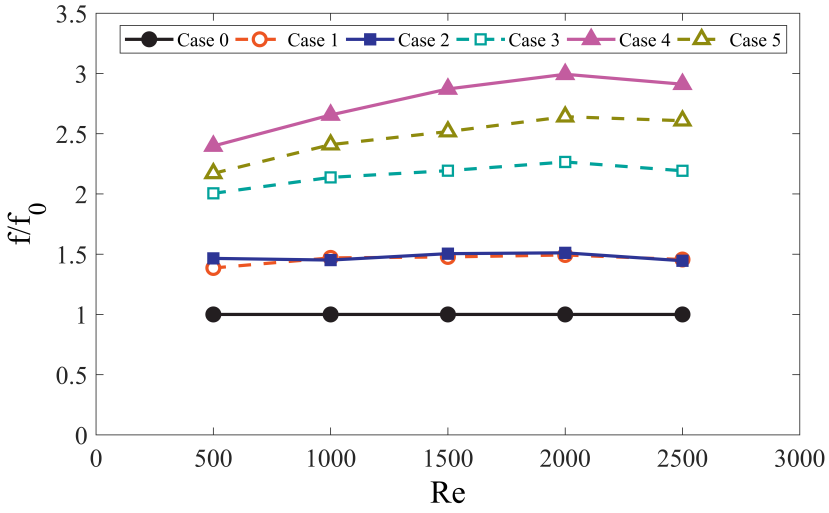

Figure 4.35: Ratio between friction factors and Case 0 friction factor.

For an appropriate HE performance evaluation it is important to look at two parameters: Heat transfer and pressure loss. The JFw thermal-dynamic efficiency factor compared every geometry with the base case (Case 0) considering the effects of heat transfer and the associated pressure loss. The best performance for every Reynolds studied is achieved in Case 5, despite the fact that Case 4 showed a better average Nusselt (Figure 4.36). The results obtained for the JFw factor suggest that the geometries selected after having reviewed the existing literature were, in fact, correct. Every geometry showed a better performance than the preceding design for every Reynolds number. As expected, performance increases for lower Reynolds. The difference between the JFw factor in Case 4 and 5 is more substantial for lower Reynolds and converge into a value for Reynolds 2500 of 1.6 approximately. Finally, the best performance is found in Case 5 for a Reynolds of 1500, where the JFw factor is 1.9 times bigger than the base case.

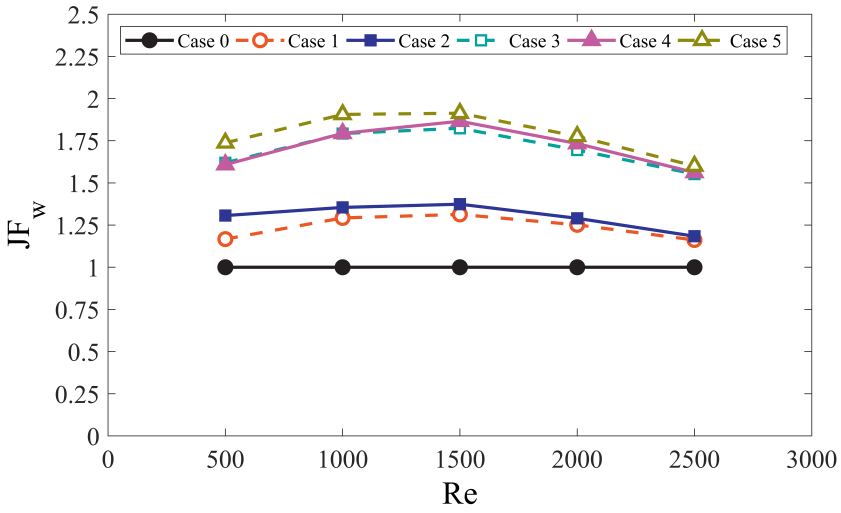

Figure 4.36: JFw for different cases.

For a practical approach, power was charted as a function of input velocity as seen in Figure 4.37. It is worth mentioning that a similar pattern was observed in all the cases: the higher the input velocity, the higher the power consumed. Case 2, corresponding to staggered tubes with oval shape, obtained lower values when compared to the rest of the cases. And Case 1, because of the staggered circular tube bank, presents similar values than the case with a pair of DWVGs. Even though cases 4 and 5 have the same heat transfer surface area, together with the same inlet velocities, Case 5 with a CFU-CFD DWVG orientation exhibits lower power due to a lower pressure drop which translates into lower costs.

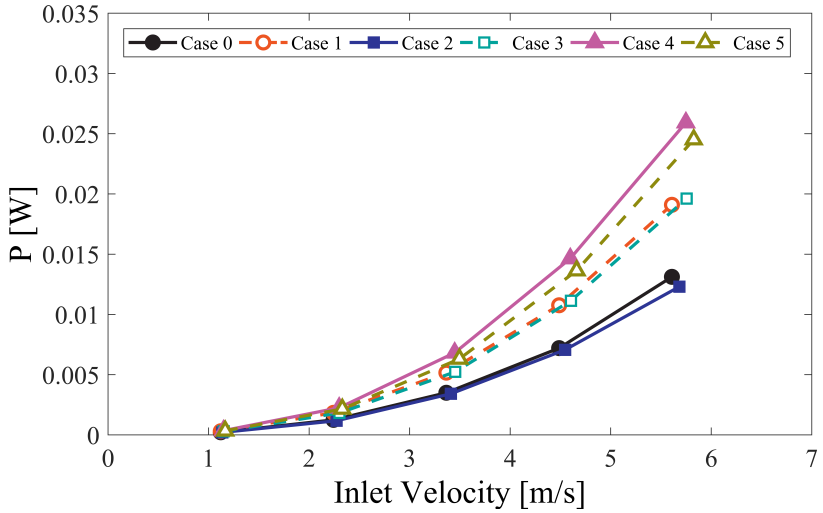

Figure 4.37: Hydraulic Power for different inlet velocities.

Finally, a graph including heat transfer rate and hydraulic power was made to compare the cases, as seen in Figure 4.38. If Case 1 is compared with Case 2, this is staggered circular tubes and staggered oval-shaped tubes, Case 1 displays a lower heat transfer rate while consuming more power for all the Reynolds (up to 56% more than Case 2) because of the different input velocities that originate from the use of the hydraulic diameter. Thus,

these results depend on the used criteria. Then, if a pair of DWVGs (Case 3) are added, the consumed power increases up to 60% (compared to cases without DWVGs) but the heat transfer rate rises significantly, reaching 38% more for Reynolds above 2000. Lastly, it is interesting to note that if cases 4 and 5 are compared, the latter shows a lower power consumption for all the studied Reynolds, reaching 8% less for Reynolds 1500 with a slight difference in heat transfer rate (less than 3.7%). This result confirms the values obtained from the JFw factor, thus concluding that Case 5 has the best performance.

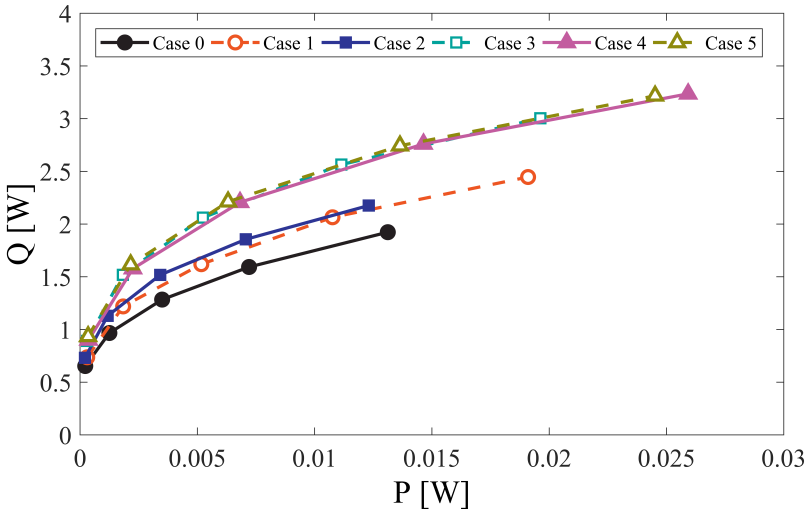

Figure 4.38: Heat transfer rate versus hydraulic power.

Chapter 5

Conclusions

The purpose of this study was to quantify and compare the thermohydraulic performance of the proposed TFHEs designs based on preliminary studies. Each new configuration was more complex and offered a better performance than the previous ones presented. The HE configuration that exhibited the best performance was the final design: TFHE with staggered oval tubes and two pairs of DWVGs in CFU-CFD orientation (Case 5). When compared with the base case (Case 0, in-line circular tubes), the final design showed an enhancement of 90% in the thermal performance factor. Consequently, the objective of this study was accomplished as Case 5 corresponds to the final configuration which suggested the best performance according to the literature review.

Every new design configuration had an effect on the flow behaviour and with each TFHE the heat transfer was enhanced. The staggered arrangement improved the mix flow in dead water zones -recirculation zones- because every tube guided the flow to the wake of the preceding tube. Oval tubes showed a better performance than circular tubes. Although the pressure loss was noticeably similar between them, the heat transfer was superior for the oval tubes by reason of a smaller stagnation zone. Finally, the addition of DWVGs showed the highest impact on the flow. Indeed, the implementation of one pair of VGs per tube increased the JFw by 30% in the HE with staggered oval tubes and a pair of DWVGs (Case 3) compared to the previous design which did not have any VGs (Case 2). This was possible thanks to the LVs generated characterized by a better fluid mix and interruption of boundary layers which achieve a better temperature distribution.

Even though staggered oval tubes with two pairs of DWVGs in CFD-CFD orientation (Case 4) exhibited the best average Nusselt number with a Reynolds of 1500 -260% higher than the base case- the generated vortices also increased the pressure loss reaching a superior loss than Case 5, where fewer but stronger vortices were identified. The best performance is a balance between heat transfer and pressure loss.

The thermal performance increased respect of the base design in all of the cases with a Reynolds number lower than 1500. In fact, the Case 5's JFw factor was 90% higher than the base case. As it was expected and supported by previous research suggesting that passive techniques for heat transfer enhancement were more efficient for lower inlet velocities (in this case 1500 Reynolds or lower).

As previously mentioned, the best performance in every case was achieved with a Reynolds number of 1500. Further research could examine or introduce a new configuration that enhances performance by means of passive techniques focusing on the study of a fixed Reynolds of 1500.

Bibliography

[1] W. S. Chang and L. W. 1994. Swanson. *Fundamentals of Heat Pipes.*

[2] Dusan P. Sekulic. *Compact heat exchangers.* 2018.

[3] M. 1998. Fiebig. Vortices, generators and heat transfer. *Chemical Engineering Research and Design*, 76(2):108–123.

[4] M. Fiebig. Vortices and heat transfer. *ZAMM Zeitschrift fur Angewandte Mathematik und Mechanik. 1997.*, 77(1):3–18.

[5] Lei Chai and Savvas A. 2018. Tassou. A review of airside heat transfer augmentation with vortex generators on heat transfer surface. *Energies*, 11(10).

[6] G. Biswas, K. Torii, D. Fujii, and K. 1996. Nishino. Numerical and experimental determination of flow structure and heat transfer effects of longitudinal vortices in a channel flow. *International Journal of Heat and Mass Transfer*, 39(16):3441–3451.

[7] M. Fiebig, A. Valencia, and N. K. 1993. Mitra. Wing-type vortex generators for fin-and-tube heat exchangers. *Experimental Thermal and Fluid Science*, 7(4):287–295.

[8] K. M. Kwak, K. Torii, and K. 2002. Nishino. Heat transfer and flow characteristics of fin-tube bundles with and without winglet-type vortex generators. *Experiments in Fluids*, 33(5):696–702.

[9] K. Torii, K. M. Kwak, and K. 2002. Nishino. Heat transfer enhancement accompanying pressure-loss reduction with winglet-type vortex generators for fin-tube heat exchangers. *International Journal of Heat and Mass Transfer*, 45(18):3795–3801.

[10] K. M. Kwak, K. Torii, and K. 2003. Nishino. Heat transfer and pressure loss penalty for the number of tube rows of staggered finned-tube bundles with a single transverse row of winglets. *International Journal of Heat and Mass Transfer*, 46(1):175–180.

[11] K. M. Kwak, K. Torii, and K. 2005. Nishino. Simultaneous heat transfer enhancement and pressure loss reduction for finned-tube bundles with the first or two transverse rows of built-in winglets. *Experimental Thermal and Fluid Science*, 29(5):625–632.

[12] A. Valencia M. Fiebig and N. Mitra. 1994. Local heat transfer and flow losses in fin-and-tube heat exchangers with vortex generators: A comparison of round and flat tubes. *Experimental Thermal and Fluid Science*, 8(1):35–45.

[13] Hui Han, Ya Ling He, Yin Shi Li, Yu Wang, and Ming. 2013. Wu. A numerical study on compact enhanced fin-and-tube heat exchangers with oval and circular tube configurations. *International Journal of Heat and Mass Transfer*, 65:686–695.

[14] M. C. Gentry and A. M. 2002. Jacobi. Heat transfer enhancement by delta-wing-

generated tip vortices in flat-plate and developing channel flows. *Journal of Heat Transfer*, 124(6):1158–1168.

[15] Daniel Díaz and Alvaro. 2017. Valencia. Heat transfer in an oval tube heat exchanger with different kinds of longitudinal vortex generators. *Heat Transfer Research*, 48(18):1707–1725.

[16] J. M. Wu and W. Q. 2012. Tao. Effect of longitudinal vortex generator on heat transfer in rectangular channels. *Applied Thermal Engineering*, 37:67–72.

[17] J. M. Wu and W. Q. 2007. Tao. Investigation on laminar convection heat transfer in fin-and-tube heat exchanger in aligned arrangement with longitudinal vortex generator from the viewpoint of field synergy principle. *Applied Thermal Engineering*, 27(14-15):2609–2617.

[18] Yong Gang Lei, Ya Ling He, Li Ting Tian, Pan Chu, and Wen Quan. 2010. Tao. Hydrodynamics and heat transfer characteristics of a novel heat exchanger with delta-winglet vortex generators. *Chemical Engineering Science*, 65(5):1551–1562.

[19] P. Chu, Y. L. He, Y. G. Lei, L. T. Tian, and R. 2009. Li. Three-dimensional numerical study on fin-and-oval-tube heat exchanger with longitudinal vortex generators. *Applied Thermal Engineering*, 29(5-6):859–876.

[20] Y. L. He, H. Han, W. Q. Tao, and Y. W. 2012. Zhang. Numerical study of heat-transfer enhancement by punched winglet-type vortex generator arrays in fin-and-tube heat exchangers. *International Journal of Heat and Mass Transfer*, 55(21-22):5449–5458.

[21] S. Tiwari, D. Maurya, G. Biswas, and V. 2003. Eswaran. Heat transfer enhancement in cross-flow heat exchangers using oval tubes and multiple delta winglets. *International Journal of Heat and Mass Transfer*, 46(15):2841–2856.

[22] Li Ting Tian, Ya Ling He, Yong Gang Lei, and Wen Quan. 2009 Tao. Numerical study of fluid flow and heat transfer in a flat-plate channel with longitudinal vortex generators by applying field synergy principle analysis. *International Communications in Heat and Mass Transfer*, 36(2):111–120.

[23] Anupam Sinha, K. Ashoke Raman, Himadri Chattopadhyay, and Gautam. 2013. Biswas. Effects of different orientations of winglet arrays on the performance of plate-fin heat exchangers. *International Journal of Heat and Mass Transfer*, 57(1):202–214.

[24] Y. Chen, M. Fiebig, and N. K. 2000. Mitra. Heat transfer enhancement of finned oval tubes with staggered punched longitudinal vortex generators. *International Journal of Heat and Mass Transfer*, 43(3):417–435.

[25] S. M. Pesteei, P. M.V. Subbarao, and R. S. 2005. Agarwal. Experimental study of the effect of winglet location on heat transfer enhancement and pressure drop in fin-tube heat exchangers. *Applied Thermal Engineering*, 25(11-12):1684–1696.

[26] Muhammad Awais and Arafat A. 2018. Bhuiyan. Heat transfer enhancement using different types of vortex generators (VGs): A review on experimental and numerical activities. *Thermal Science and Engineering Progress*, 5:524–545.

[27] Ya Ling He and Yuwen Zhang. *Advances and Outlooks of Heat Transfer Enhancement by Longitudinal Vortex Generators*, volume 44. Elsevier.

[28] Carpio Contreras. 2019. Aumento de la transferencia de calor mediante generadores de vórtices longitudinales en intercambiadores de calor compacto. *Memoria de Ingeniero Civil Mecánico. Santiago, Universidad de Chile, Facultad de Ciencias Físicas y Matemáticas.*

Appendix A

Grid Independence

Table A.1: Heat transfer coefficient and friction factor comparison.

Mesh	Re	h [W/m^{2}K]	f	Error h [%]	Error f [%]
Coarse Mesh	600	45.56	0.0808	0.0	-0.8
	1,400	62.75	0.0550	-4.0	-4.8
	2,200	83.85	0.0465	-2.7	-0.9
Medium Mesh	600	46.67	0.0819	2.4	0.7
	1,400	63.41	0.0569	-3.0	-1.5
	2,200	86.15	0.0465	0.0	-0.8
Fine Mesh	600	45.56	0.0814	-	-
	1,400	65.35	0.0578	-	-
	2,200	86.15	0.0469	-	-

Table A.2: Average skewness and mean orthogonal quality.

Category	Coarse Mesh	Medium Mesh	Fine Mesh
Average Skewness	0.1849	0.1817	0.1718
Average Orthogonal Quality	0.8179	0.8180	0.8296

Appendix B

Inlet Velocities

Table B.1: Inlet velocities for every configuration.

Re	Case 0	Case 1	Case 2	Case 3	Case 4	Case 5
500	1.121	1.121	1.136	1.151	1.149	1.165
1000	2.243	2.243	2.273	2.302	2.299	2.330
1500	3.365	3.365	3.410	3.453	3.448	3.495
2000	4.487	4.487	4.546	4.604	4.598	4.661
2500	5.609	5.609	5.683	5.755	5.748	5.826

Appendix C

Results Obtained

Table C.1: Results obtained for Case 0.

Re	T_{in} [K]	T_{out} [K]	ΔP [Pa]	$\dot{m}$ [kg/s]
500	293.00	304.62	4.84	0.00005593
1,000	293.00	301.59	13.71	0.00011187
1,500	293.00	300.61	25.59	0.00016781
2,000	293.00	300.08	39.51	0.00022374
2,500	293.00	299.84	57.55	0.00027966

Table C.2: Results obtained for Case 1.

Re	T_{in} [K]	T_{out} [K]	ΔP [Pa]	$\dot{m}$ [kg/s]
500	293.00	306.15	6.71	0.00005568
1,000	293.00	303.87	20.15	0.00011149
1,500	293.00	302.62	37.80	0.00016732
2,000	293.00	302.20	59.02	0.00022316
2,500	293.00	301.72	83.79	0.00027901

Table C.3: Results obtained for Case 2.

Re	T_{in} [K]	T_{out} [K]	ΔP [Pa]	$\dot{m}$ [kg/s]
500	293.00	305.93	4.54	0.00005627
1,000	293.00	303.12	12.74	0.00011095
1,500	293.00	301.91	24.65	0.00016927
2,000	293.00	301.17	38.24	0.00022576
2,500	293.00	300.66	53.28	0.00028231

Table C.4: Results obtained for Case 3.

Re	T_{in} [K]	T_{out} [K]	ΔP [Pa]	$\dot{m}$ [kg/s]
500	293.00	308.46	6.46	0.00005736
1,000	293.00	306.16	19.49	0.00011471
1,500	293.00	304.91	37.31	0.00017206
2,000	293.00	304.11	59.53	0.00022945
2,500	293.00	303.41	83.90	0.00028689

Table C.5: Results obtained for Case 4.

Re	T_{in} [K]	T_{out} [K]	ΔP [Pa]	$\dot{m}$ [kg/s]
500	293.00	308.70	7.69	0.00005703
1,000	293.00	306.73	24.12	0.00011420
1,500	293.00	305.80	48.66	0.00017133
2,000	293.00	304.98	78.36	0.00022908
2,500	293.00	304.23	110.98	0.00028637

Table C.6: Results obtained for Case 5.

Re	T_{in} [K]	T_{out} [K]	ΔP [Pa]	$\dot{m}$ [kg/s]
500	293.00	309.01	7.25	0.00005806
1,000	293.00	306.84	22.79	0.00011609
1,500	293.00	305.63	44.42	0.00017411
2,000	293.00	304.76	72.00	0.00023193
2,500	293.00	304.02	103.54	0.00029006

Table C.7: Nu with Equation 3.20 and Nuspan with Equation 3.19

Case	Re	Nu	Nuspan	Relative Difference Nu [%]
Case 0	500	4.84	4.65	-3.9
	1,000	6.25	5.94	-5.0
	1,500	7.99	7.29	-8.7
	2,000	9.72	9.14	-6.0
	2,500	11.64	11.48	-1.4
Case 1	500	5.93	6.05	1.9
	1,000	8.69	8.72	0.3
	1,500	10.92	10.90	-0.2
	2,000	13.67	13.08	-4.4
	2,500	15.89	15.11	-4.9
Case 2	500	6.66	6.90	3.5
	1,000	9.03	9.11	0.8
	1,500	11.53	11.47	-0.5
	2,000	13.68	13.53	-1.1
	2,500	15.74	15.37	-2.4
Case 3	500	9.44	9.49	0.5
	1,000	13.67	13.71	0.3
	1,500	17.29	17.27	-0.1
	2,000	20.66	20.35	-1.5
	2,500	23.42	23.15	-1.1
Case 4	500	9.77	10.01	2.4
	1,000	14.76	14.75	-0.1
	1,500	19.50	19.33	-0.9
	2,000	23.30	22.83	-2.0
	2,500	26.30	25.60	-2.7
Case 5	500	10.53	10.46	-0.7
	1,000	15.39	15.17	-1.4
	1,500	19.57	18.97	-3.1
	2,000	23.15	22.44	-3.1
	2,500	26.16	25.28	-3.4

Table C.8: JFw calculated.

Re	Case 0	Case 1	Case 2	Case 3	Case 4	Case 5
500	1.000	1.167	1.306	1.619	1.608	1.738
1,000	1.000	1.292	1.355	1.793	1.794	1.906
1,500	1.000	1.313	1.374	1.824	1.866	1.913
2,000	1.000	1.251	1.290	1.695	1.733	1.776
2,500	1.000	1.162	1.184	1.552	1.562	1.600

Appendix D

Contours

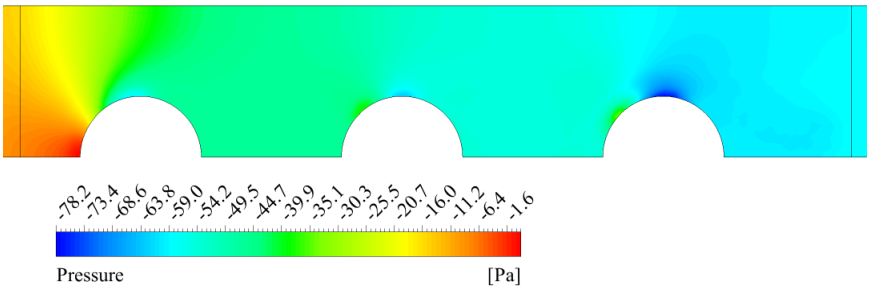

Figure D.1: Total pressure contour for Case 0.

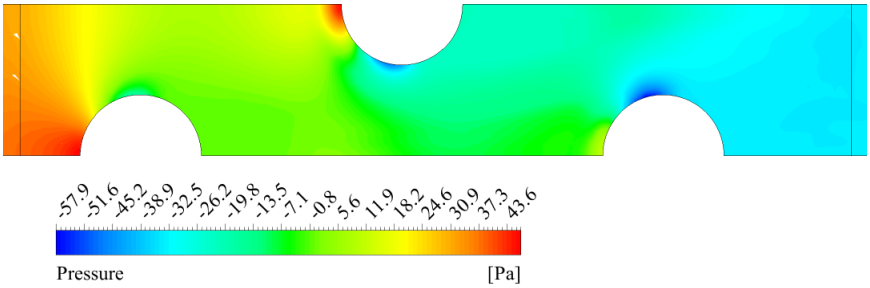

Figure D.2: Total pressure contour for Case 1.

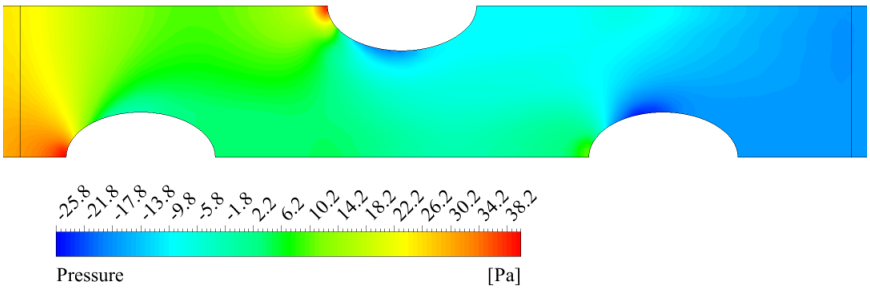

Figure D.3: Total pressure contour for Case 2.

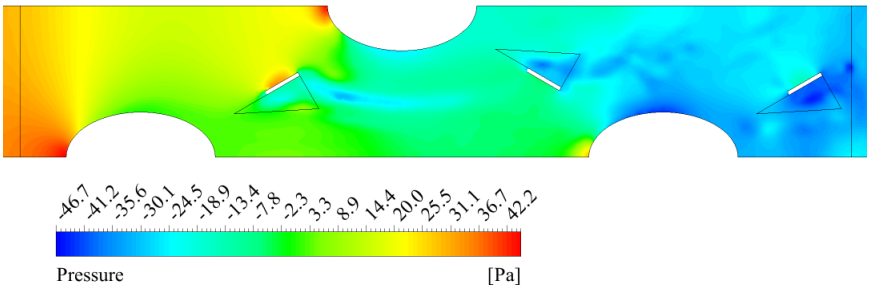

Figure D.4: Total pressure contour for Case 3.

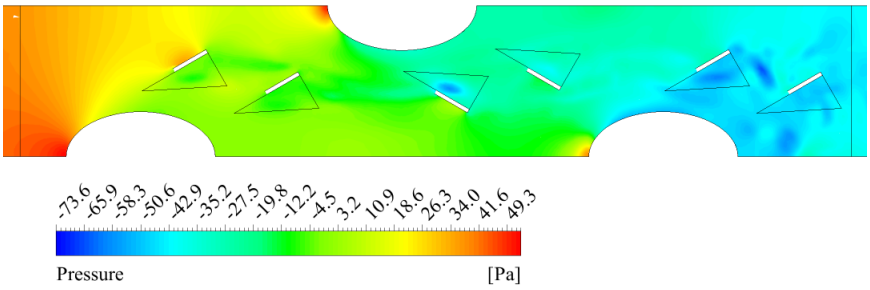

Figure D.5: Total pressure contour for Case 4.

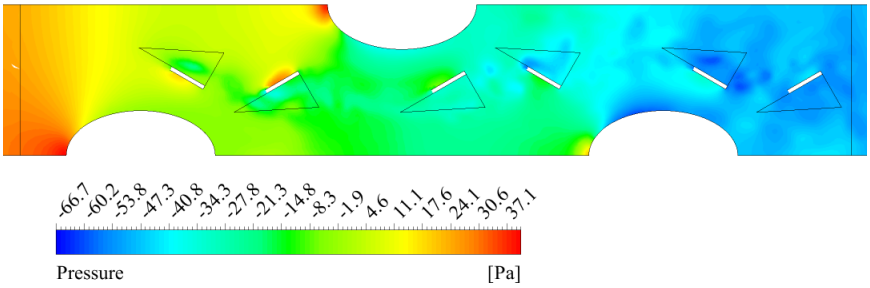

Figure D.6: Total pressure contour for Case 5.

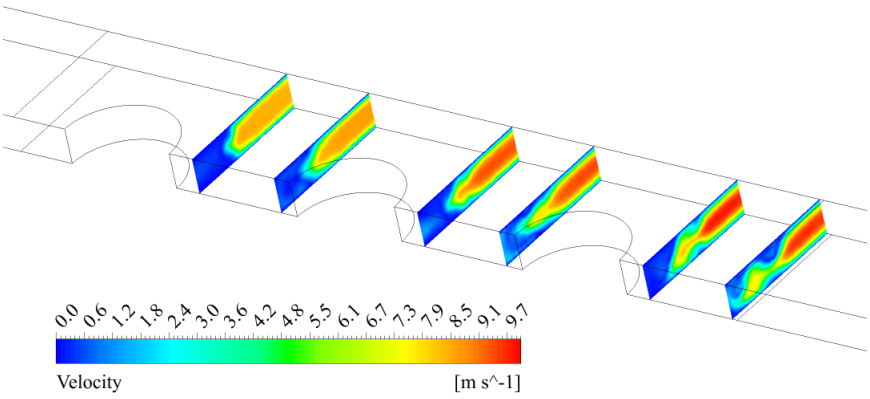

Figure D.7: Velocity profile in different planes for Case 0.

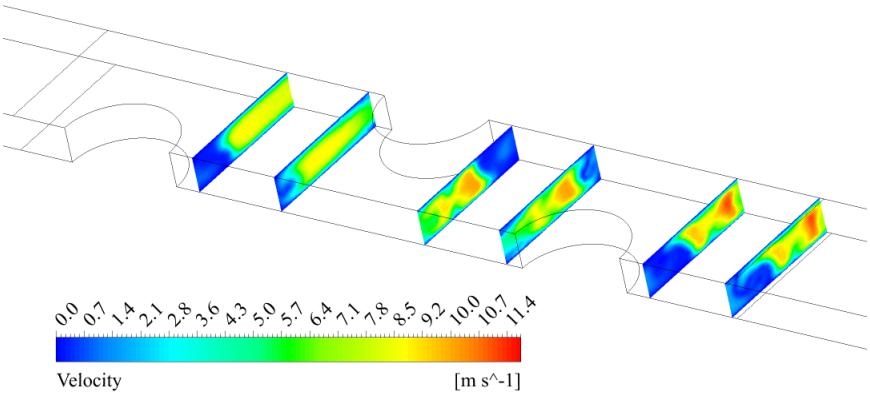

Figure D.8: Velocity profile in different planes for Case 1.

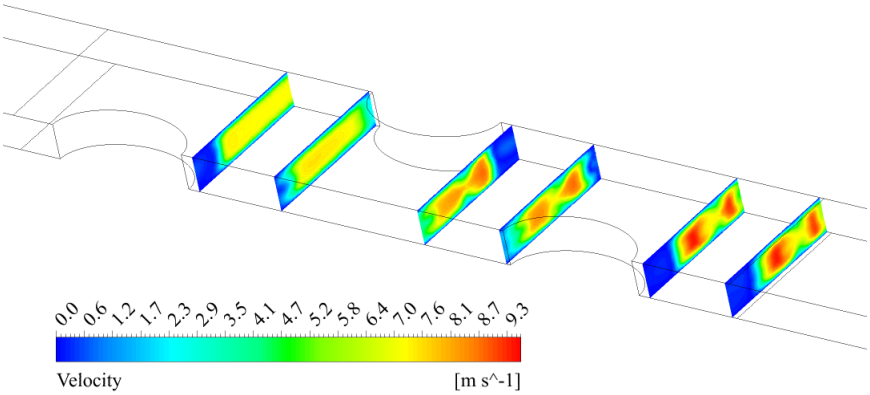

Figure D.9: Velocity profile in different planes for Case 2.

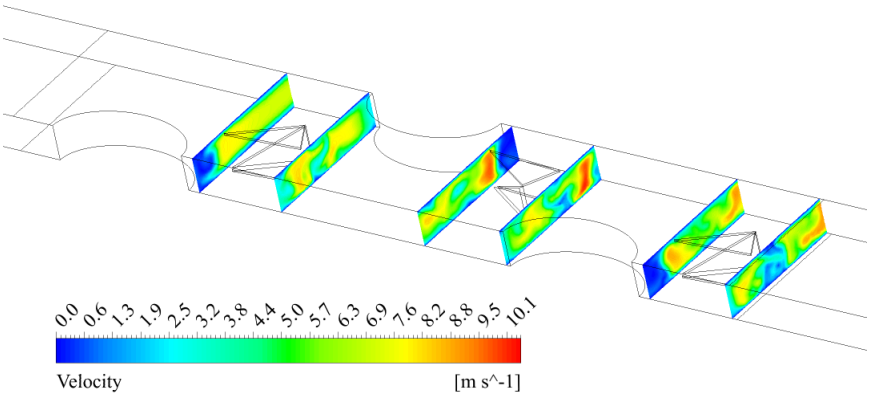

Figure D.10: Velocity profile in different planes for Case 3.

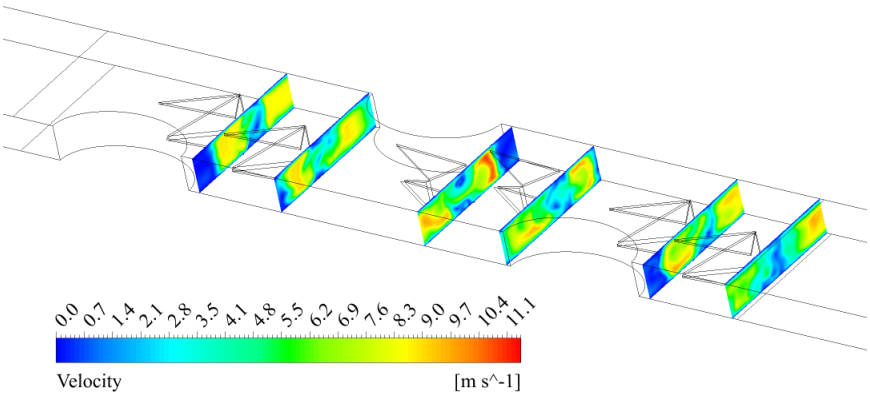

Figure D.11: Velocity profile in different planes for Case 4.

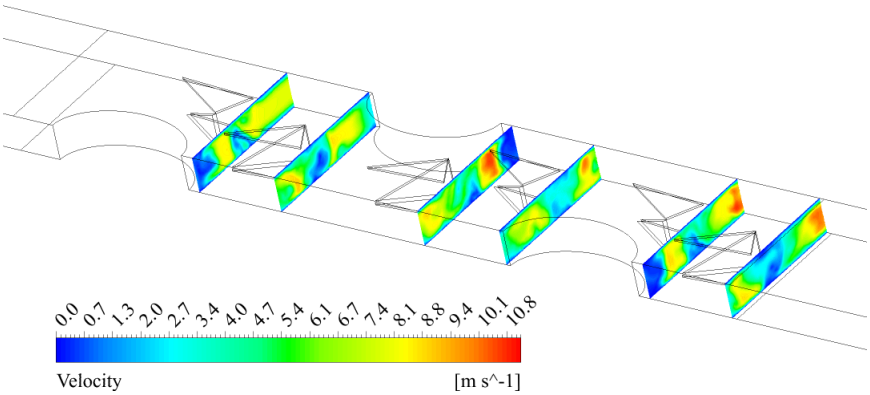

Figure D.12: Velocity profile in different planes for Case 5.

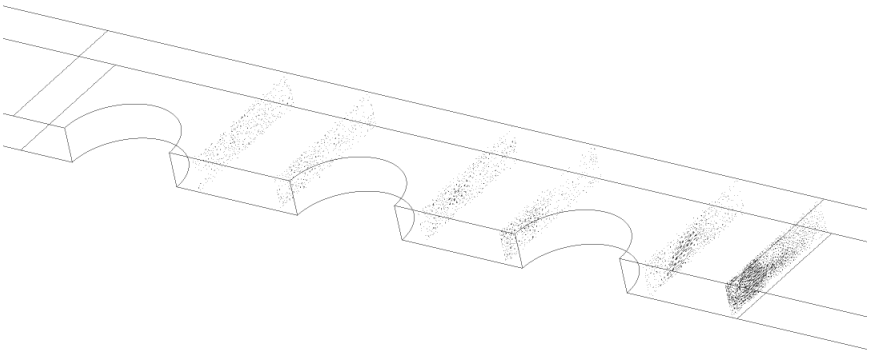

Figure D.13: Velocity vectors in different planes for Case 0.

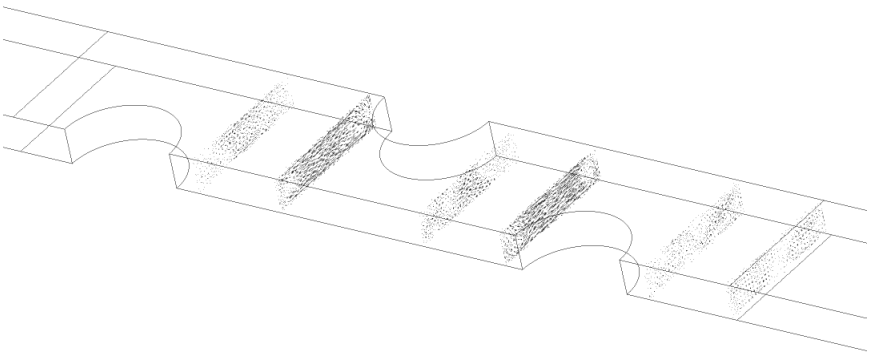

Figure D.14: Velocity vectors in different planes for Case 1.

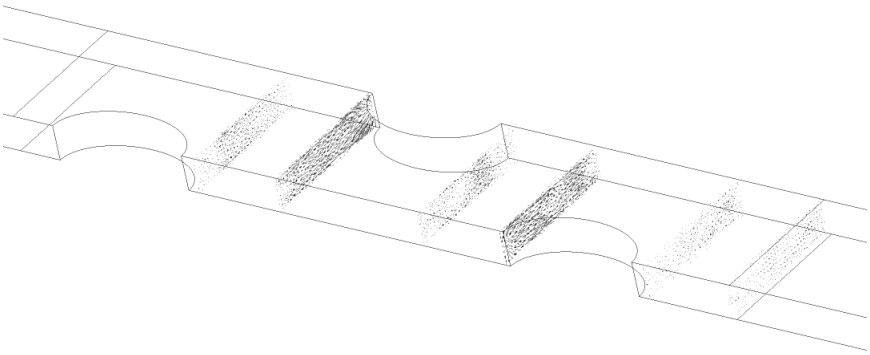

Figure D.15: Velocity vectors in different planes for Case 2.

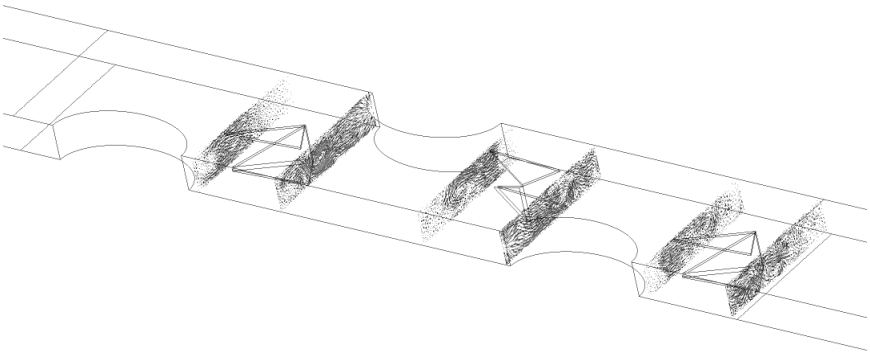

Figure D.16: Velocity vectors in different planes for Case 3.

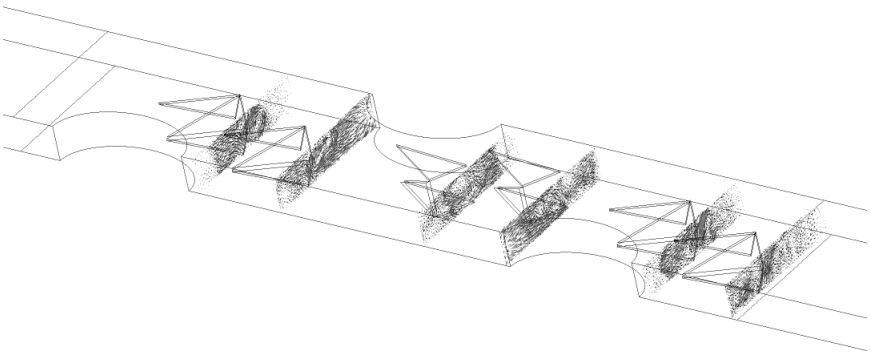

Figure D.17: Velocity vectors in different planes for Case 4.

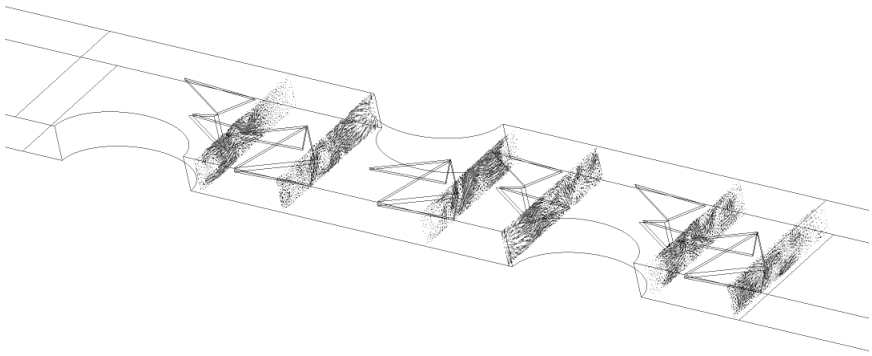

Figure D.18: Velocity vectors in different planes for Case 5.

Appendix E

Span average Nusselt number code.

Code E.1: Span average Nusselt number code [28].

```
USER SCALAR VARIABLE:  TmprVel
Boundary Values = Conservative
Calculate Global Range = Off
Expression = Temperature*Velocity u
Recipe = Expression
Variable to Copy = Pressure
Variable to Gradient = Pressure
END

!CreateSectionPlanes();
! sub CreateSectionPlanes{

! $PlanePreName = "Plane YZ ";
! $LinePreName = "Line";


! $PlotVariable1 = "TmprVel";
! $PlotVariable2 = "Velocity u";
! $PlotVariable3 = "Temperature";
! $PlotVariable4 = "Wall Heat Flux";


! $CalcFunction1 = "areaAve($PlotVariable1)";
! $CalcFunction2 = "areaAve($PlotVariable2)";
! $CalcFunction3 = "lengthAve($PlotVariable3)";
! $CalcFunction4 = "areaAve($PlotVariable4)";


! $MinVal = 0;
! $MaxVal = 0.5;


! $startX =-0.01014;
! $startY = 0;
```

```
! $startZ = 0;


!$startX1 = -0.01014;
!$startY1 = 0;
!$startZ1 =0;


!$startX2 =0.05986;
!$startY2 = 0;
!$startZ2 =0;


! $dX = 0.000066;
! $dY = 0;
! $dZ = 0;


! $TotalNo = 1001;


! open(SwRes,">D:\Archivos\CC.csv") || die "Can't open file $!\n";
#Escribe la primera fila del cvs
! print SwRes "Plane , X , Y , Z ,"  ,$CalcFunction1, "," ,$CalcFunction2 , ","  ,"Line ,
    ↪ X1 , Y1 , Z1 , X2 , Y2 , Z2 ",  ","  ,$CalcFunction3 ,  ","  ,$CalcFunction4 , "\n";


! for ($j=0; $j<$TotalNo ;$j++) {


! $PlaneName = $PlanePreName . ($j+1);
! $LineName = $LinePreName . ($j+1);


! $NewX = $startX + $dX * $j;
! $NewY = $startY + $dY * $j;
! $NewZ = $startZ + $dZ * $j;


! $NewX1 = $startX1 + $dX * $j;
! $NewY1 = $startY1 + $dY * $j;
! $NewZ1 = $startZ1 + $dZ * $j;


! $NewX2 = $startX2 + $dX * $j;
! $NewY2 = $startY2 + $dY * $j;
! $NewZ2 = $startZ2 + $dZ * $j;


! $CalcString1 = $CalcFunction1 . "@" . $PlaneName;
```

```
! $CalcString2 = $CalcFunction2 . "@" . $PlaneName;
! $CalcString3 = $CalcFunction3. "@" . $LineName;
! $CalcString4 = $CalcFunction4. "@" . $PlaneName;


PLANE: $PlaneName
Apply Instancing Transform = On
Apply Texture = Off
Blend Texture = On
Bound Radius = 0.5 [m]
Colour = 0.75, 0.75, 0.75
Colour Map = Default Colour Map
Colour Mode = Variable
Colour Scale = Linear
Colour Variable = $PlotVariable2
Colour Variable Boundary Values = Hybrid
Culling Mode = No Culling
Direction 1 Bound = 1.0 [m]
Direction 1 Orientation = 0 [degree]
Direction 1 Points = 10
Direction 2 Bound = 1.0 [m]
Direction 2 Points = 10
Domain List = /DOMAIN GROUP:All Domains
Draw Faces = On
Draw Lines = Off
Instancing Transform = /DEFAULT INSTANCE TRANSFORM: Default Transform
Invert Plane Bound = Off
Lighting = Off
Line Colour = 0, 0, 0
Line Colour Mode = Default
Line Width = 1
Max = $MaxVal
Min = $MinVal
Normal = 1 , 0 , 0


Option = YZ Plane

Plane Bound = None
Plane Type = Slice
Point = 0 [m], 0 [m], 0 [m]
Point 1 = 0 [m], 0 [m], 0 [m]
Point 2 = 1 [m], 0 [m], 0 [m]
Point 3 = 0 [m], 1 [m], 0 [m]
Range = User Specified
Render Edge Angle = 0 [degree]
Specular Lighting = On
Surface Drawing = Smooth Shading
Texture Angle = 0
Texture Direction = 0 , 1 , 0
```

```
Texture File =
Texture Material = Metal
Texture Position = 0 , 0
Texture Scale = 1
Texture Type = Predefined
Tile Texture = Off
Transform Texture = Off
Transparency = 0.0
 Visibility  = On


X = $NewX
Y = $NewY
Z = $NewZ
OBJECT VIEW TRANSFORM:
Apply Reflection = Off
Apply Rotation = Off
Apply Scale = Off
Apply Translation = Off
Principal Axis = Z
Reflection Plane Option = XY Plane
Rotation Angle = 0.0 [degree]
Rotation Axis From = 0 [m], 0 [m], 0 [m]
Rotation Axis To = 0 [m], 0 [m], 0 [m]
Rotation Axis Type = Principal Axis
Scale Vector = 1 , 1 , 1
Translation Vector = 0 [m], 0 [m], 0 [m]
X = 0.0 [m]
Y = 0.0 [m]
Z = 0.0 [m]
END
END


LINE: $LineName
  Apply Instancing Transform = On
  Colour = 1, 1, 0
  Colour Map = Default Colour Map
  Colour Mode = Constant
  Colour Scale = Linear
  Colour Variable = $PlotVariable3
  Colour Variable Boundary Values = Conservative
  Domain List = /DOMAIN GROUP:All Domains
  Instancing Transform = /DEFAULT INSTANCE TRANSFORM:Default Transform
  Line Samples = 10
  Line Type = Cut
  Line Width = 2
  Max = $MaxVal
  Min = $MinVal

```

```
184
185   Option = Two Points
186   Point 1 = $NewX1, $NewY1, $NewZ1
187   Point 2 = $NewX2, $NewY2, $NewZ2
188   Range = Global
189    Visibility  = On
190   OBJECT VIEW TRANSFORM:
191     Apply Reflection = Off
192     Apply Rotation = Off
193     Apply Scale = Off
194     Apply Translation = Off
195     Principal  Axis = Z
196     Reflection  Plane Option = XY Plane
197     Rotation Angle = 0.0 [degree]
198     Rotation Axis From = 0 [m], 0 [m], 0 [m]
199     Rotation Axis To = 0 [m], 0 [m], 0 [m]
200     Rotation Axis Type = Principal Axis
201     Scale  Vector = 1 , 1 , 1
202     Translation  Vector = 0 [m], 0 [m], 0 [m]
203     X = 0.0 [m]
204     Y = 0.0 [m]
205     Z = 0.0 [m]
206   END
207 END
208
209
210
211 ! $CalcVal1 = getExprVal($CalcString1);
212 ! $CalcVal2 = getExprVal($CalcString2);
213 ! $CalcVal3 = getExprVal($CalcString3);
214 ! $CalcVal4 = getExprVal($CalcString4);
215 ! print  SwRes $PlaneName, " , " ,$NewX, " , " ,$NewY, " , " ,$NewZ, " , "  ,$CalcVal1, "  ,
      ↪ "  ,$CalcVal2, "  ,  "  ,$LineName, " , "  ,$NewX1," , ",$NewY1," , ",$NewZ1," ,
      ↪ ",$NewX2," , ",$NewY2," , ",$NewZ2, "," ,$CalcVal3, ","  ,$CalcVal4, "\n";
216
217 ! };
218
219 !  close  SwRes;
220 !};
```